Desalination and Water Treatment
www.deswater.com

doi: 10.5004/dwt.2018.23132

135 (2018) 25–46
December

Thermal analysis and optimization of mechanical vapour compression desalination process driven by renewable energy using genetic algorithm

M. Ghazi[a,b,*], M. Faqir[a], M. Mada[b], E. Essadiqi[a]

[a]*LERMA Laboratory, International University of Rabat Sale, Morocco, e-mail: ghazimohamed.emi@gmail.com (M. Ghazi), elhachmi.essadiqi@uir.ac.ma (E. Essadiqi), mustapha.faqir@uir.ac.ma (M. Faqir)*
[b]*Ecole Mohammadia d'Ingénieurs, ITACS Lab, Rabat, Morocco, e-mail: mada@emi.ac.ma (M. Mada)*

Received 13 April 2018; Accepted 13 September 2018

ABSTRACT

In this work, a seawater desalination unit using mechanical vapour compression process driven by a hybrid Wind-Photovoltaic energy system is studied and optimized using genetic algorithm optimization method. The developed model is based on mass and energy balance equations, heat transfer correlations and thermodynamic properties of each stream. The study takes into account the effect of design parameters and the impact of operating conditions. The developed model is validated based on the experimental data of similar process published in literature. The obtained results show that when using one effect, the optimal cost of produced distilled water is approximately equal to 4.2 US$/m^3 for a production capacity equal to 5 m^3/d and achieves an optimal value equals to 2.5 US$/m^3 when the production capacity ranges between 100 and 120 m^3/d. Also, results show that the optimal cost of produced distilled water could be less than 0.77 US$/m^3 for a production capacity equal to 1000 m^3/day and when the number of effects is equal to 8 which is close to the average cost of water production in Morocco. At the end of this study, further possible improvements of the optimized design are proposed based on energy efficiency analysis.

Keywords: Seawater desalination; Mechanical vapour compression; Multi effect evaporation; Hybrid wind-solar energy; Optimization and design; Exergy analysis

1. Introduction

Seawater desalination technologies are considered as very promising solution to deal with the continuous increase of water demand in the world, especially on countries that suffer from water shortage. Desalination processes could be classified into two categories: thermal and membrane methods. Thermal processes that are based on phase change include the multi stage flash process, multi effect evaporation, and humidification/dehumidification process. These processes require a large amount of thermal energy. However, membrane processes are generally based on the use of electrical or mechanical energy required to drive the power machines. Mechanical vapour compression is considered as one of the most attractive among various desalination processes, especially when combined with renewable energy technologies. The first and the only one desalination MVC unit was built in Morocco in 1977 with a production capacity equals to 250 m^3/d. Its shut-down at 1995 was because of its limited capacity and its high specific energy consumption [1]. In the literature, the most published papers deal with the thermal analysis, the thermo-economical and the economic study, design, optimization and the performance evaluation of the existent MVC units. Some studies also deal with the study and analysis of the combination of MVC desalination process and the use of renewable energy technologies. One of the first published papers dealing with the economic study of the MVC system is the work published by Matz and Fisher [2] in 1980, they compared the economic performance of MVC and RO desalination processes based on the power consumption and they found; at that time, that the total cost could be closed for both technologies because of the high cost related to membranes replacement and intensive chemical treatment for the RO process, which result in comparable total product cost for both systems.

*Corresponding author.

After that, several papers are published on the thermal analysis, modelling, exergy analysis and simulation of single effect and multi-effect MVC systems [3–13], these papers studied the impact of design parameters and the operating parameters, such as: the compression ratio, the top brine temperature and the feed seawater intake temperature on the system performance such as the specific power consumption, the phase change specific heat transfer area, and the recovery heat exchangers performance. Their studies are based on Material and energy balance equations and thermodynamics and physical correlations. In this regard, the most relevant results and conclusions made by the authors are:

- The energy consumption could be reduced by combining the VC with MSF or MED.
- The exergy lost could be decreased by increasing the number of effect and decreasing the TBT.
- The power consumption decreases when the temperature difference decreases while the specific heat transfer area increases.
- The specific power consumption and specific area decreases at higher top brine temperature and the power consumption decreases when the temperature difference decreases while the specific heat transfer area increases.
- High top brine temperature decreases the compression power consumption and the heat transfer area however it increases the fouling and corrosion problems.

Other published papers studied and described the characteristics and performance of existent units. In 1985, Lucas and Tabourier [14] presented the characteristics of MVC unit combined with four effect multi stage technology which was the biggest of that type installed in the world with a production capacity of 1500 t/d installed in France. So far, several existent units are also presented and described in the literature [15–20]. The conclusions made from these papers concerning the advantages of using MVC process and the practical improvements are as follow:

- High energy savings, reliability and long lifetime due to the use of durable construction materials such as Aluminium, Titanium and Copper-Nickel (90/10) tubes, plastic piping and Epoxy painted steel shells.
- Prevention of scaling and corrosion problems by using low temperatures and using horizontal tubes falling evaporators technology;
- Compactness which reduces the transportation and erection costs;
- The MVC technology requires simple seawater intake without particular pre-treatment; and provides high product purity from any kind of seawater.

Also, several papers are published on the economic analysis and evaluation of water production cost using MVC technology and its comparison with the other technologies. El-Sayed [21] stated that research and development could decrease the water cost by 30% while increasing the MVC unit efficiency by 50%.

However, in the literature, there is a wide dispersion in determining the water cost using MVC technology because there is no unified design of the existent units and some costs were not accounted such as pre-treatment and land cost, in addition there is a wide difference in terms of the material and energy cost. Indeed, Khayet [22], in his paper dealing with dispersion in energy consumption analysis and water production costs, found that the MVC water production cost ranges between 0.46 and 1.21 US$/m^3. The latest published works give more interest on integrating and combining the MVC desalination units with renewable energy technologies. The most suitable technologies to be combined with MVC desalination technology are PV panels, wind turbine, and solar thermal power cycles. Helal and Al Malek [20] designed a new solar assisted mechanical vapour compression unit with a production capacity of 120 m^3/d, they provided the optimal design for the global unit which allows the cost reduction and saves the disposal of approximately 160 t/y of CO_2. Sharaf et al. [11] evaluate and analysed a combined multi effect distillation-vapour compression unit, in their work, two solar technologies are taken into account: in the first one the solar field is used to generate steam which is used directly to drive the desalination unit based on the thermal compression process and in the second one solar organic Rankine cycle is used to convert the solar thermal energy into electrical power in order to drive mechanical vapour compression unit. They also found that the reduction of the compression ratio and increasing the number of effects reduce the specific power consumption.

Zejli et al. [23] presented hybrid photovoltaic wind system to drive a MVC desalination plant with storage unit; they formulated an optimization problem taken into account three specific case studies in Morocco in order to ensure a variable hourly and monthly domestic water demand, their results show that water demand could be satisfied with a cost comparable to the average cost of water in Morocco which is equal to about 0.8 US$/m^3.

The International University of Rabat proposed the construction of new pilot seawater desalination unit based on using mechanical vapour compression process and renewable energy technologies. The aim of this study is to demonstrate the feasibility and effectiveness of such technology and to prove that this combination is very promising in terms of cost and pollutant reduction especially for Moroccan deserted regions. This paper is divided into five sections; the first one is dedicated to providing a detailed description of the process and the principle characteristics of each component and device, the second section presents the developed model of equations and describes the resolution and optimization algorithm, the third section is devoted to thermal and economic analysis of single effect MVC desalination process, the fourth section presents and discusses the optimal results concerning the case of using multi-effect MVC desalination process, and finally, in the fifth section, the exergy efficiency analysis is carried out for additional improvements of the optimized design.

The hybrid energy renewable energy system optimization methodology and the estimation of the electrical energy cost are provided in Appendix 1. The heat transfer correlations, thermodynamics properties, and

cost estimation of different equipment are also given in Appendix 2, 3, 4 and 5.

2. Process description and material selection

The considered mechanical vapour compression seawater desalination unit is composed of four major parts as shown in Fig. 1: Energy production system, evaporation/condensation unit, heat recovery heat exchangers and other auxiliary equipment such as storage tanks, pumps and the process control system. A hybrid solar-wind energy system is used to provide the unit with the required thermal and electrical energy; it is composed of solar vacuum tubes thermal panels, photovoltaic panels and wind turbines. The evaporation/condensation unit consists of a series of evaporators maintained in parallel configuration; each evaporator is made of a temperature resistant food-compatible plastic container, and equipped with a series of parallel-submerged coils made of special salt water resistant copper-nickel tube. The last effect is combined with a vapour compressor. An additional series of coils are added at bottom of the first effect in order to complete the feed seawater heating to achieve the saturated state and to compensate the decrease of latent heat caused by the augmentation of pressure. During the steady-state operation of the unit, a portion of feed seawater is evaporated inside each evaporator under reduced pressure; the produced steam is forced inside the following evaporator where it is used as heating medium and then releasing its latent heat of condensation. The produced vapour at the last effect passes through the compressor where its pressure is increased, so the steam is superheated and then forced inside the first evaporator coils. Condensation takes place and once more the released latent heat is transferred to the feed seawater. To minimize the energy consumption two plate heat exchangers are used for heat recovery from brine and distilled water. The technical characteristics of wind turbines and solar panels used in the hybrid energy system are given in the Appendix 1. The hybrid PV-Wind energy system is designed in order to insure more that 60% of fossil fuel replacement rate, fossil fuel energy (energy from the up-grid or diesel generator) will be used only in the case of renewable energy insufficiency. A detailed design, sizing and optimization study of the hybrid PV-Wind energy system is provided in the Appendix 1 based on weather conditions of Layouune region (33°39′58″ N, 7°04′16″ W).

3. Modelling equations

3.1. Heat exchangers

The feed seawater is pumped from the storage tank at T_0 and forced through the adjustable flow divider; the first portion of the feed seawater (m_{f1}) is pre-heated by the brine via the plate heat exchanger 1, the other portion (m_{f2}) is heated by the distilled water using the plate heat exchanger 2.

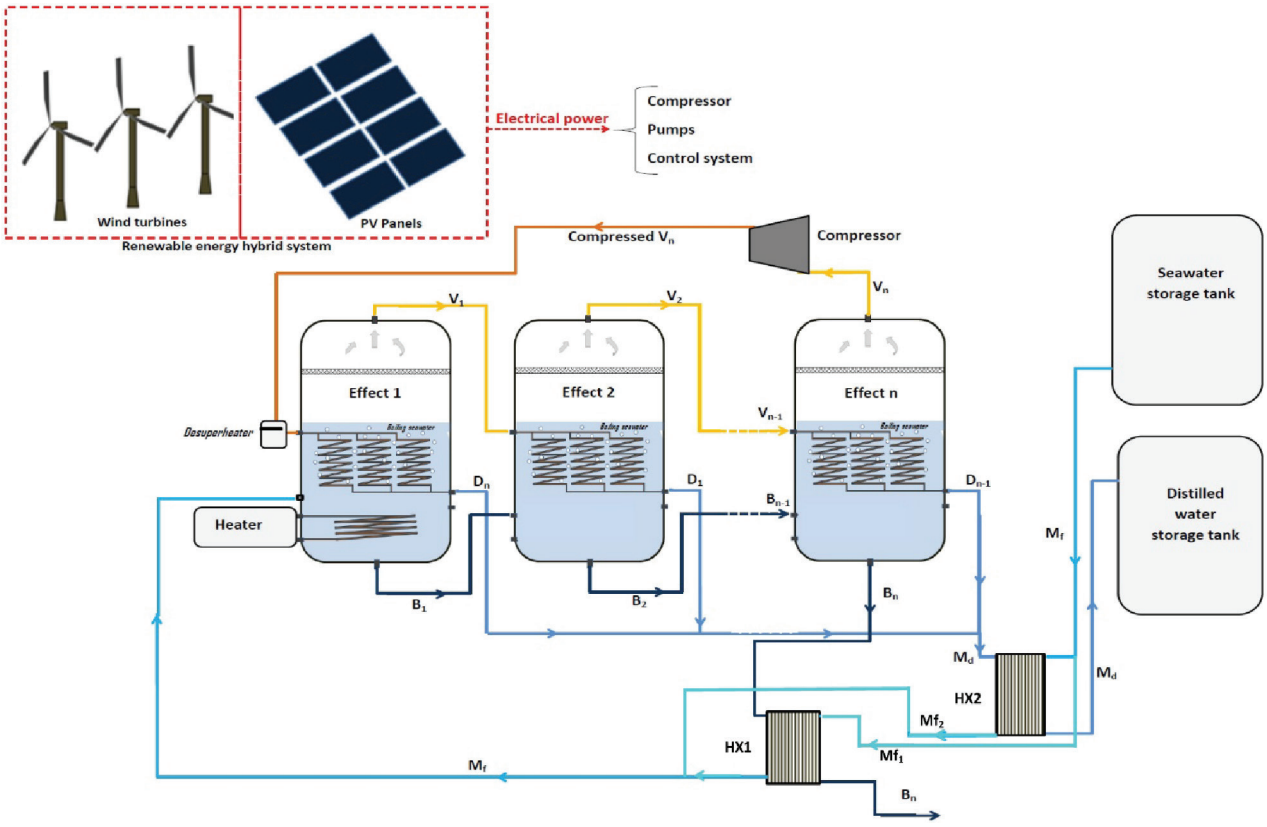

Fig. 1. Solar driven MVC unit.

The heat gained through the heat recovery system by seawater is calculated using the following equations:

The mass balance equations:

$$\dot{m}_f = \dot{m}_b + \dot{m}_d = \dot{m}_{f1} + \dot{m}_{f2} \tag{1}$$

$$\dot{m}_d = X\dot{m}_f \tag{2}$$

$$\dot{m}_{f1} = \alpha\dot{m}_f \tag{3}$$

The heat balance equations

$$Q_r = Q_{r1} + Q_{r2} = \dot{m}_f c_f \left(T_f - T_0\right) \tag{4}$$

$$Q_{r1} = \dot{m}_{f1} c_f \left(T_{f1} - T_0\right) + Q_{los,r1} = \dot{m}_b c_b \left(T_b - T_{b0}\right) \tag{5}$$

$$Q_{r2} = \dot{m}_{f2} c_f \left(T_{f2} - T_0\right) + Q_{los,r2} = \dot{m}_d c_d \left(T_d - T_{d0}\right) \tag{6}$$

Heat transfer equations

$$Q_{r1} = U_{r1} A_{r1} LMTD_{r1} \tag{7}$$

$$Q_{r2} = U_{r2} A_{r2} LMTD_{r2} \tag{8}$$

The correlations and the calculation method for the global heat transfer coefficients for the plate heat exchangers, the log mean temperature difference and the specific thermal capacities are given in the appendix with details.

3.2. Mechanical vapour compression system

3.2.1. For the first effect

As mentioned before, heating of feed seawater is completed using a series of coils located at the bottom of the first evaporator in order to achieve the boiling temperature and starting the formation of small amount of vapour which compensates the decrease of the latent heat when the pressure increases, the required energy is provided by solar vacuum tube collectors using hot water as heating medium, the heating thermal power is expressed by the following equation:

$$\dot{Q}_h = \dot{M}_f c_{sw} \left(T_{boiling} - T_f\right) + \dot{m}'_d L_{evap}\left(T_1\right) = \dot{m}_s c_s \left(T_s - T_{s0}\right) \tag{9}$$

Heat transfer equations

$$Q_h = U_h A_h LMTD_h \tag{10}$$

As the feed seawater heats, it expands slightly and becomes lighter and flows naturally to the above part of the evaporator where the second group of coils are located. Then, saturated feed seawater starts boiling by exchanging the latent heat with the condensing compressed vapour flowing inside the coils. The heat exchanged during this process is calculated using the equation:

$$\dot{Q}_1 = \left(\dot{V}_1 - \dot{V}'_1\right) L_{evap}\left(T_1\right) = \dot{V}_n L_{cond}\left(T_{comp}\right) \tag{11}$$

Heat transfer equation is expressed by:

$$\dot{Q}_1 = U_1 A_1 \left(T_{comp} - T_1\right) \tag{12}$$

3.2. Effect number 'i' (i > 1)

Each effect is driven by low pressure steam produced in the previous effect, thus, the mass flow rate of vapour formed using the latent heat is calculated using equation:

$$\dot{Q}_i = \dot{V}'_i L_{evap}\left(T_i\right) = \dot{V}_{i-1} L_{cond}\left(T_{i-1}\right) \tag{13}$$

The portion of vapour produced by free boiling or flash process of brine inside each evaporator could be estimated by equation:

$$V''_i = B_{i-1} c_{sw} \left(T_{i-1} - T_i\right) \Big/ L_{evap}\left(T_i\right) \tag{14}$$

The total amount of vapour produce inside each effect is determined using equation:

$$V_i = V'_i + V''_i \tag{15}$$

The boiling heat transfer equation is expressed by the following equation:

$$\dot{Q}_i = U_i A_i \left(T_{i-1} - T_i\right) \tag{16}$$

3.3. Compression process

The produced vapour in the last effect is forced inside the compressor where its pressure increased, consequently, its temperature increased, at the outlet of the compressor a small amount of saturated water is injected using spray process in order to transform the superheated produced vapour to saturated vapour which led to avoiding the inconvenient of low heat transfer coefficient of superheated vapour inside the coil. The electrical energy needed to drive the compressor is assumed using the relationship:

$$\dot{Q}_{comp} = \dot{V}_n \frac{\gamma}{(\gamma - 1)\eta_c} P_n v_n \left(\left(\frac{P_{comp}}{P_n} \right)^{\frac{\gamma - 1}{\gamma}} - 1 \right) \tag{17}$$

A detailed correlations and assumptions used to estimate the heat transfer coefficients are given in appendix.

4. Sizing and optimization algorithm

The schematic of the developed resolution and optimization algorithm is presented in Fig. 2. It is based on both fixed point iterations methodology and genetic algorithm optimization method. Fixed point iteration method is used in order to resolve the highly non-linear equations developed in the previous section while genetic algorithm is implemented in order to find out the most optimal configuration of the unit in terms of design and operating conditions leading minimizing the cost of

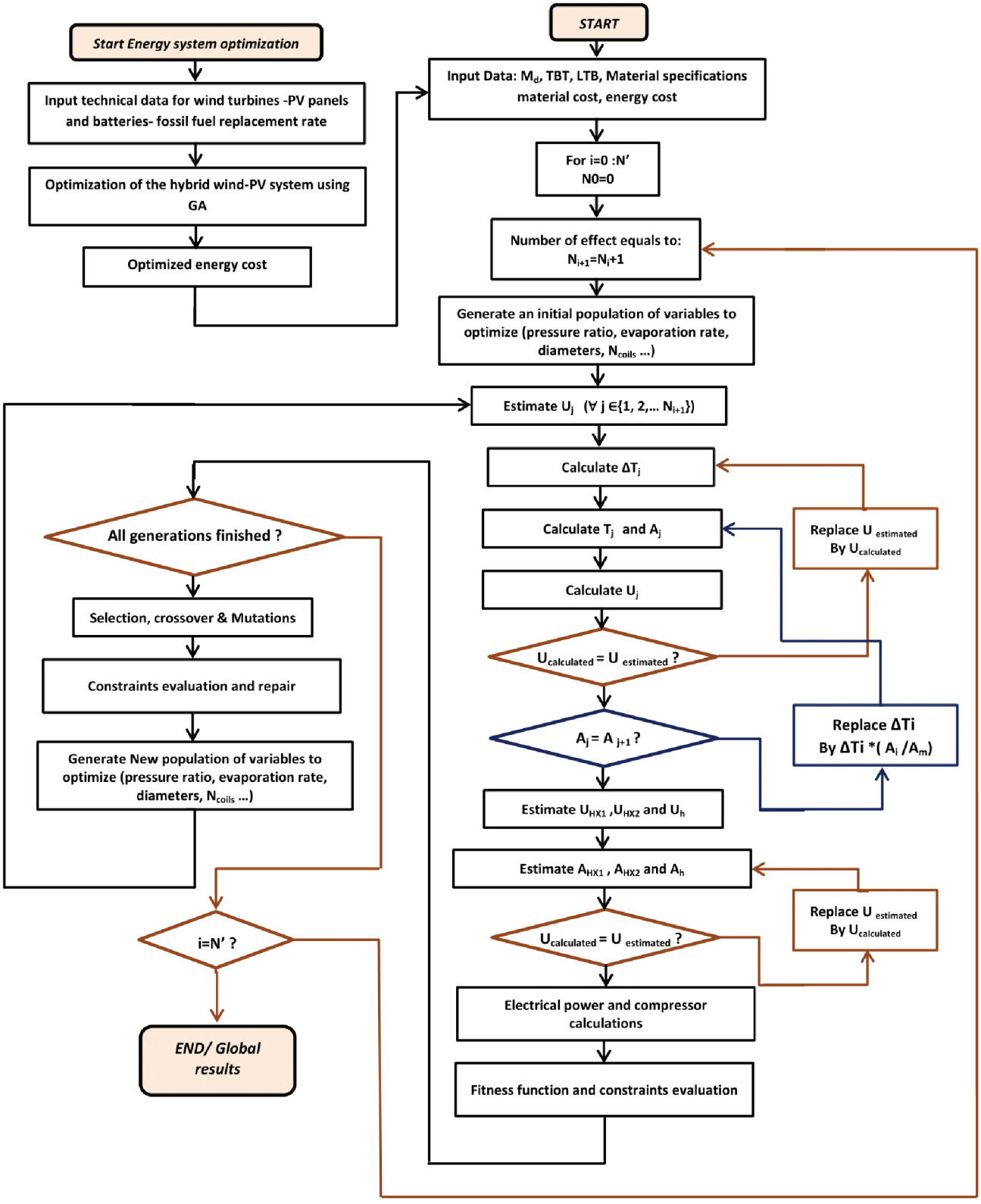

Fig. 2. Developed computational algorithm.

produced distilled water. In the optimization procedure, nine different variables have been taken into consideration, which are: pressure ratio of the compressor, evaporation rate, top brine temperature, tubes diameter, coils diameter and number of parallel coils in addition to dimensions of the palate heat exchangers that will be used for heat

recovery. The optimization procedure is applied to different numbers of effects (ranging between 1 and 14) and for different production capacities (5, 10, 100, 1000 m^3/d). The algorithm start by generating an initial population of variables to optimize for N_i-effects desalination unit, and used as input for the sizing-calculation loop using fixed iterations method. In the developed algorithm, initially, the evaporators-heat transfer coefficients are estimated and then used to calculate the temperature difference between condensing vapour and boiling seawater for each effect using equal thermal load assumption. After that, the temperature and the heat transfer area are calculated for each effect; in that case, new values of the overall heat transfer coefficients are calculated and compared with the assumed values, if the difference between each assumed value and the new calculated one exceeds the tolerance value (0.001), the estimated values are replaced by the calculated values and then the same iteration is repeated until achieving the convergence criteria. Next, the equality of the heat transfer area is checked; if the error is greater than the tolerance value, the temperature difference ΔTj in each effect will be corrected by the ratio of the calculated heat transfer area and its average value for all the effects. This procedure is followed by calculating the required heat transfer area of the plate heat exchangers and the heating area for the first effect based on using fixed point iteration method, the next step in the algorithm is to determine the electrical power consumed by the compressor. At this stage, all parameters related to evaporators, heat recovery heat exchangers and the compressor are computed and then the following step is the fitness function evaluation for each feasible solution in the selected population of variables. The fitness function is water production cost in (US$/$m^3$), which is expressed in terms of the annual amortized total cost and the annual water production capacity. The fitness function with lowest value compared to the value obtained from the previous iterations is considered as an initial optimal solution of the optimization algorithm. The initial-best solutions create the next new generation through the selection of chromosomes, crossover and mutation operations (reproduction of new generation of solutions). The same procedure is repeated until achieving the optimization convergence criteria. Also, the algorithm stops if there are no improvements of the value of the fitness function after a set number of generations. Then, the algorithm is repeated for a N_i+1-effects desalination unit until achieving the maximum number of effect N' (14 is taken as a maximum number of effects in this study). It is also worth mentioning that the energy cost is obtained from a preliminary optimization study (presented in the Appendix 1) of the hybrid PV-Wind energy system using Genetic Algorithm optimization method in order to find out the most optimal configuration of wind turbines and solar photovoltaic panels taken into account weather data of the studied location (Laayoune region-Morocco). The obtained cost of energy is taken as input data in optimization procedure of seawater desalination unit. The developed algorithm is implemented using Matlab programming software. The effectiveness of the developed sizing algorithm (based on fixed point iterations) is validated using the experimental results presented in the literature; the validation is based on comparing our modelled results with the experimental results presented by Aly et al. [18] for a single effect MVC unit of the Heat Transfer Laboratory of the Atomic Energy Authority of Egypt. As shown in Table 1, the modelled results show a good agreement with the experimental and the design parameters except for the evaporator heat transfer parameters (overall heat transfer coefficient and

Table 1
Comparison between modelled and experimental results

	Results from Ref. [18]			Model results	Error (%)
	Calculated	Design	Experimental		
T_{evap} (°C)	69.06	69.5	69.8	69.5	0.43
P_{eva}p (bar)	0.312	0.3	0.35	0.2919	16.6
P_{oultet} (bar)	0.4056	0.42	0.45	0.4087	9.18
M_b (kg/h)	321	420	415	391.9	5.57
M_d (kg/h)	309	308	210	208.44	0.74
T_f (°C)	69.42	69.5	68	62.5	8.09
T_b (°C)	24.8	25	26	25	3.85
U_{evap} (kW/m²K)	2.4	Not available	Not available	0.9399	Not available
$LMTD_{ev}$ (°C)	4.576	Not available	Not available	7.8677	Not available
A_{evp} (m^2)	17.068	Not available	Not available	18.12	Not available
A_{HX1} (m^2)	1.187	Not available	Not available	1.102	Not available
A_{HX2} (m^2)	1.523	Not available	Not available	1.901	Not available
W_{comp} (kJ/kg)	50.71	53.3	Not available	47.3	Not available
M_f (kg/h)	630	630	630	600.3	4.76
M_{f1} (kg/h)	309	245	Not available	208.44	Not available
M_{f2} (kg/h)	321	385	Not available	391.9	Not available

area) because the existent unit uses horizontal tubes falling film as heat transfer area inside the evaporator while our modelled unit uses submerged coils as heat transfer area for the evaporator.

Some experimental parameters are not available, thereupon the modelled results are compared with the design and the calculated results presented in [18], these parameters include the heat transfer area for the heat recovery heat exchangers, the compressor energy consumption, and the feed mass flow rate. Also, this comparison shows good agreement between our model and the published results, thus, the error does not exceed 6.7% for the heat recovery heat exchangers 1, and 1.24% for the heat exchanger 2, and it does not exceed 6.72% for the compressor specific energy consumption and 4.76%, 16%, 1.79% for the feed mass flow rate *Mf*, Mf_1 and Mf_2, respectively.

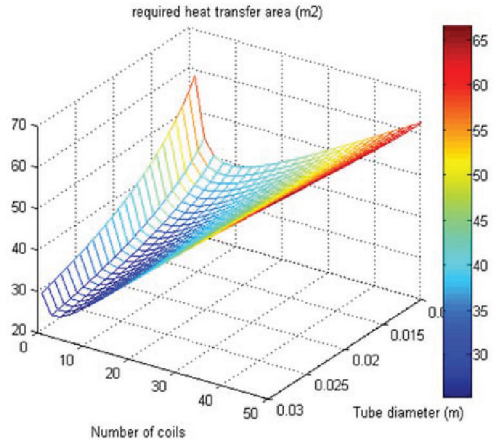

Fig. 3. The required heat transfer area vs coils diameter and tube diameter.

5. Single effect-MVC unit: thermal and economic analysis

We recall that the present study takes into account the impact; on the unit performance; of the design variables (tubes diameter, number of parallel coils and the dimensions of the plates) and the operating variables (compression ratio, top brine temperature and evaporation rate). In this section, we are considering the impact of variables indicated above on economic and thermal performance for single effect-MVC process. Thus, this section is divided into three parts, the first one deals with the analysis of the interactions between the design parameters and the unit performance, the second part is dedicated to the study of the impact of the operating parameters, and the third part is devoted to presenting the economic analysis of the unit depending on the design and operating parameters, in addition to their effect on the global cost of fresh water production. Finally, the fourth part presents the optimal results obtained for different production capacities.

The objective of this section is ensuring a better understanding of the impact degree of each parameter on the unit performance and evaluating the global performance of single effect-MVC unit.

5.1. Impact of design parameters

The design parameters, which are taken into account in this study, are the number of parallel coils used inside the evaporator and their diameter. These parameters have direct impact into the heat transfer rate but they don't affect the rate of energy required to drive the unit. Parameters related to the heat recovery heat exchangers are also studied and optimized but not included in this part. All the results and figures presented in this section are obtained for a production capacity equals to 5 m^3/d of distillate water and the evaporation rate is taken equal to 80% under vacuum at 90°C and using compressed vapour at 100.7°C.

As shown in Fig. 3, the required heat transfer area changes between 25 and 60 m^2 when the tube diameter and the number of coils change respectively between 10 and 30 mm and between 2 and 50. This result demonstrated that an appropriate selection of these parameters could decrease the evaporator heat transfer area with more than 50%. These outcomes are obtained because the overall heat transfer coefficient has also an optimum value when the number of coils is equal to 5 and for tube diameter equal 30 mm, as presented in Fig. 4, under these conditions the maximum value obtained for the overall heat transfer coefficient is equal to about 1.95 $kW/m^2/°C$. The behaviour of the overall heat transfer coefficient towards the tube diameter and the number of coils could be explained by the change of the boiling and condensing heat transfer coefficients towards the design parameters change as presented in Figs. 5 and 6. Indeed, According to Nusselt's theory [24], the heat transfer from condensing vapour to the inside-tube surface area occurs by conduction through the film of formed liquid, thus, inside the coils the condensation heat transfer rate is related to the condensate film thickness which deceases by increasing the number of coils and the tube diameter, leading then to rising the condensation heat transfer coefficient. However at the outside of coils, the boiling heat transfer coefficient decreases when the number of coils increases, and slightly increases when the tube diameter decreases.

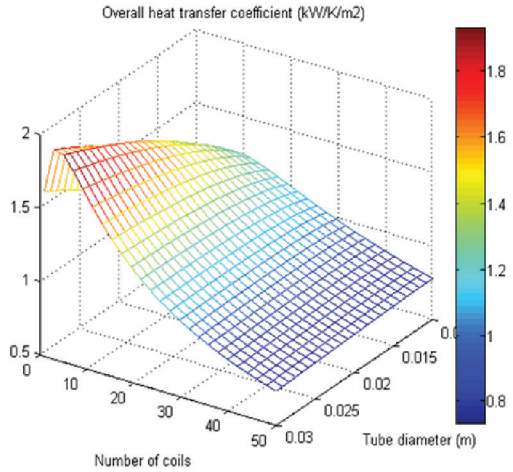

Fig. 4. The overall heat transfer coefficient vs coils diameter and tube diameter.

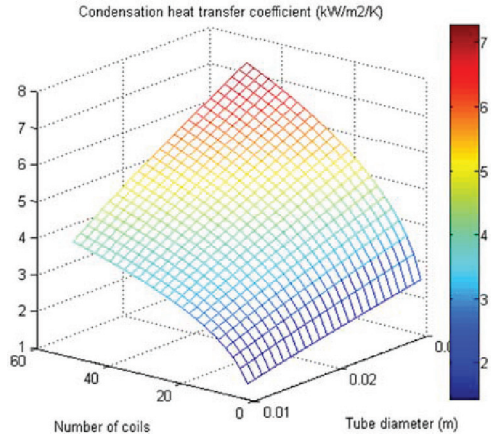

Fig. 5. The condensation heat transfer coefficient vs coils diameter and number.

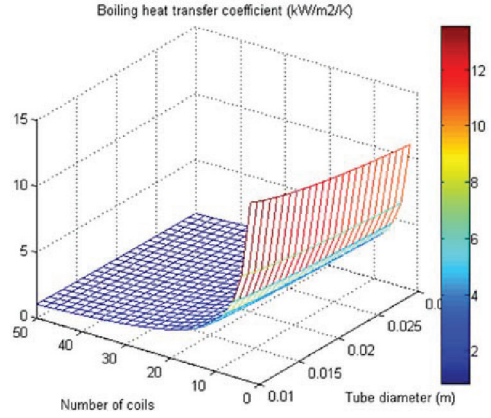

Fig. 6. The boiling heat transfer coefficient vs coils diameter and number.

Also, as shown in Figs. 7 and 8, where the production capacity is taken equal to 25 m^3/d, the effect of tube diameter is the same as the previous case, however, the optimal number of coils increases to be equal to 12 coils instead of 5 coils when the production capacity is equal to 5 m^3/d. The effect of the production capacity on the system performance is discussed in detail in the following sections dealing with the impact of operating parameters and the economic analysis.

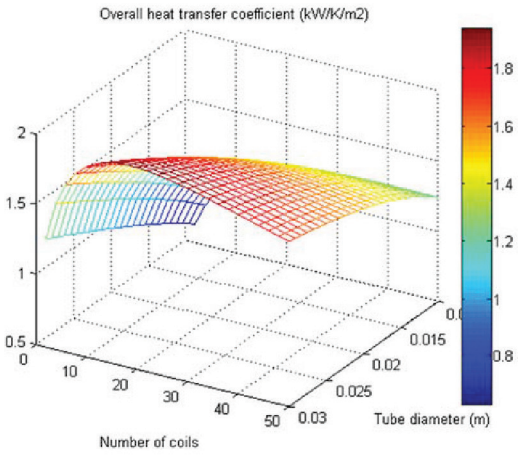

Fig. 7. The EOHTC vs coils number and tube diameter for capacity 25 m^3/d.

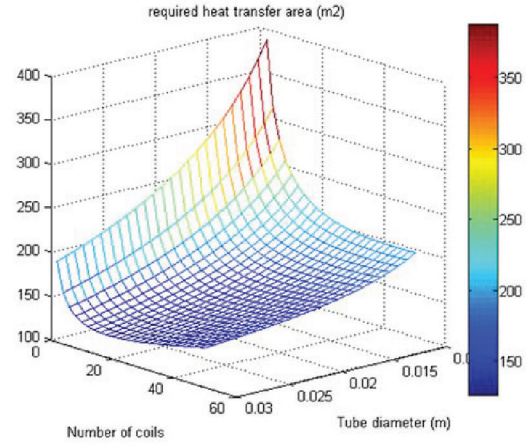

Fig. 8. The EHTA vs coils number and tube diameter for capacity 25 m^3/d.

5.2. Impact of operating parameters

The operating parameters taken into account are: the compression ratio, the boiling temperature inside the evaporator, the evaporation rate and the production capacity of the unit. This section is dedicated to studying the impact of these parameters on the compressor power consumption, the evaporator heat transfer area and the heat recovery heat exchangers performance. As shown in Fig. 9, when the compression ratio increases from 1.2 to 2.5 the required heat transfer area decreases with about 82% this is because when the compression ratio increases the temperature difference between the condensing vapour

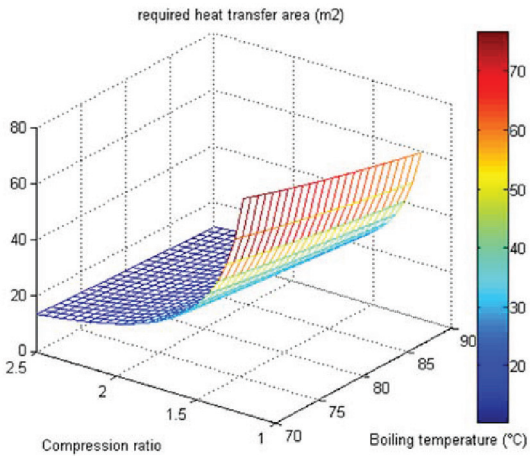

Fig. 9. The required heat transfer area vs compression ratio and boiling temperature.

and the boiling seawater increases. However, the increase of the compression ratio has a negative impact on the compressor's power consumption. Indeed, as shown in Fig. 10, when the compression ratio increases from 1.2 to 2.5 the compressor's power consumption increases with about 80%. According to Figs. 9 and 10, the boiling temperature has medium effect on the power consumption, thus, when the boiling temperature decreases from 90 to 70°C the power consumption decreases with about 10%. However, it has less effect on the required heat transfer area.

The same operating parameters have a direct impact on the heat recovery heat exchangers. We recall that plate heat exchangers are used in this unit, and the heat exchanger 1 is used for the heat exchange between the rejected brine and feed seawater and the heat exchanger 2 is used for recovering the thermal energy from the distillate leaving the evaporator. As shown in Figs. 11 and 12, the compressor ratio has no effect on the heat exchanger 1, however, when the compressor ratio increases the required heat transfer area for the heat exchanger 2 decreases. This result is obtained because when the compressor ratio increases, the condensing temperature also increases, and consequently

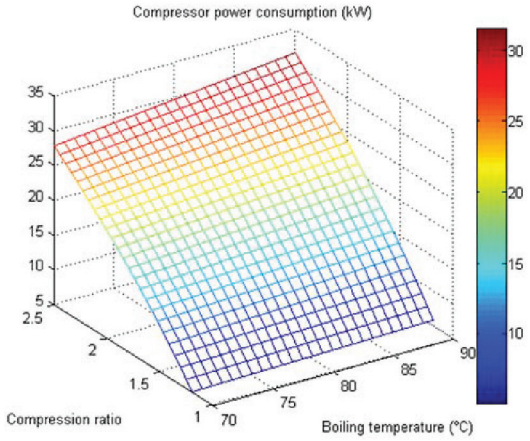

Fig. 10. The overall heat transfer coefficient vs compression ratio and boiling temperature.

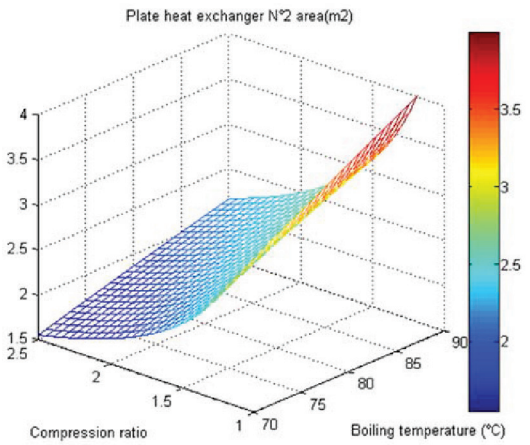

Fig. 11. P2 required heat transfer area vs compression ratio and boiling temperature.

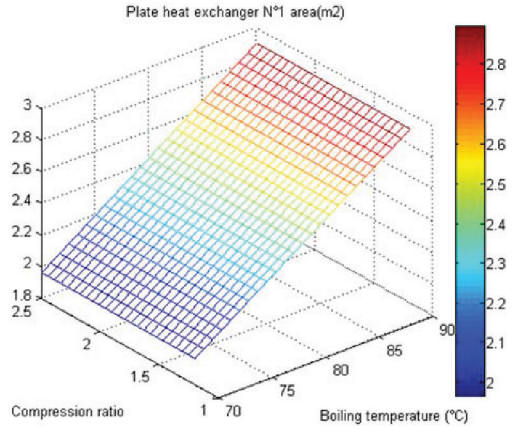

Fig. 12. P1 required heat transfer area vs compression ratio and boiling temperature.

the temperature difference between the feed seawater and the distillate water increases.

However, the boiling temperature has an opposite effect on the required heat transfer area for the heat exchangers 1 and 2, when the boiling temperature increases from 70 to 90°C, the require heat transfer area increases in both heat exchangers with more than 80% this is because in this unit the heat exchangers design is based on the feed temperature at the outlet which is directly related to the inlet temperature of the hot stream (brine and distillate). Indeed, the design model uses counter flow configuration for the heat exchangers and the difference between cold steam outlet temperature and hot stream inlet temperature is fixed and taken equal to 5°C. Thus, when the boiling temperature increases the required heat transfer area will also increase in the way that the amount of recovered heat and then the feed seawater outlet temperature meet the design requirements. Another two operating parameters that influence highly the unit performances are the evaporation rate and the production capacity. As shown in Fig. 13 the overall heat transfer coefficient could be improved not only by increasing the compression ratio but also by increasing the evaporation rate.

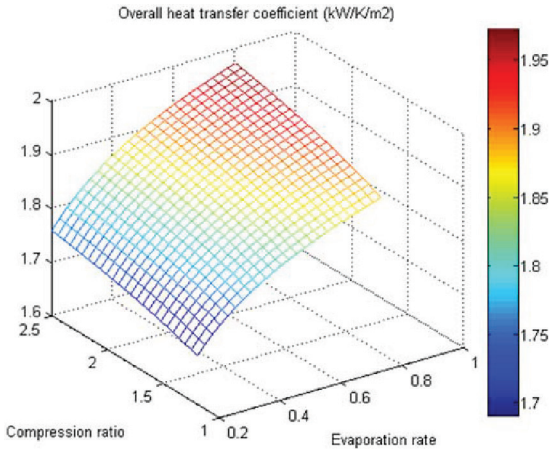

Fig. 13. The overall heat transfer coefficient vs compression ratio and evaporation rate.

Another parameter that has also a direct impact on the unit performance is the production capacity. Fig. 14 presents the simultaneous effect of the number of coils and the water production capacity on the overall heat transfer coefficient, the obtained results show that for each production capacity there a specific number of coils in which the overall heat transfer coefficient achieves its maximum value which does not exceed 1.9 kW/m^2/K.

5.3. Economic analysis

Fresh water production cost depends on several parameters that are related to design and operation of the global unit. The total cost includes the direct and indirect costs and the operating cost.

The detailed calculation of the total cost is presented in the Appendix 7 and 8. The major costs that are taken into account are the process equipment's cost such as the solar field, evaporator, compressor, heat exchangers, and storage tanks, piping and pumping system, maintenance, cleaning and manpower costs and energy cost. The unit does not use chemicals for feed seawater pre-treatment, only poor treatment is used for the produced fresh water and the feed. For these reasons, the unit operating cost takes into account only energy cost, maintenance, repairing, cleaning and manpower costs. We recall also that the economic study does not include the land cost. Fig. 15 shows that the cost passes by its minimal value which is equal to approximately 4.7 US $/m^3 when the number of parallel coils is ranging between 4 and 6 and for larger values of the tubes diameter, this is because under these conditions the required heat transfer area inside the evaporator is minimal as previously obtained in Fig. 3.

We mention that these results are obtained for: an evaporation rate of 80% of feed seawater, production capacity equals to 5 m^3/d, boiling temperature equals to T_b = 90°C and a compression ratio equals to 1.5.

As discussed in the previous parts, the change of compression rate has direct impact on the energy consumption for the compressor and also on the heat transfer area for the boiler and the heat recovery heat exchangers. Also, as shown in Fig. 16, the water production cost has a minimal value which is equal to 4.67 USD/m^3 when the compression ratio is approximately equal to 1.4 and the evaporation rate of 80%. Fig. 17 shows that the boiling temperature has less effect on the water production cost which could be decreased by increasing the production capacity of the unit. As shown in Fig. 18, distilled water cost could be less than 2.5 USD/m^3 for large production capacities.

5.4. Optimal design for single effect-MVC unit

The optimal parameters are obtained using genetic algorithm optimization method as described previously, the obtained results are presented in the following tables for four different fresh water production capacities: 5, 10, 100, and 1000 m^3/d. As mentioned before, the optimization of water cost takes into account the cost of the plate heat exchangers and the other components. Thus, the calculation results obtained for the heat recovery heat exchangers 1 and 2 are also provided. These results are obtained after a strict optimization taking into account the geometry dimensions of plates, material selection,

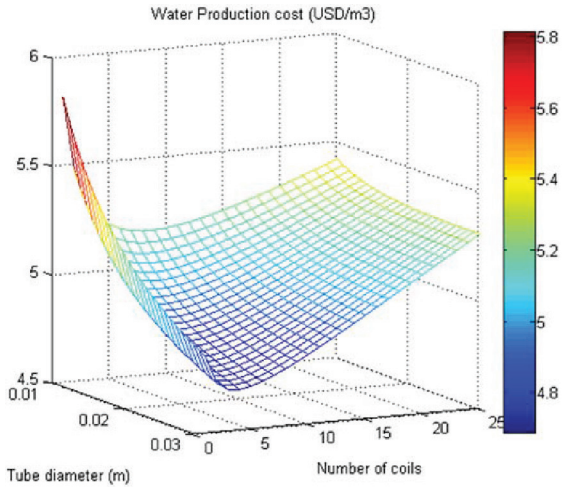

Fig. 15. Water cost (USD/m^3) vs tube diameters and number of coils.

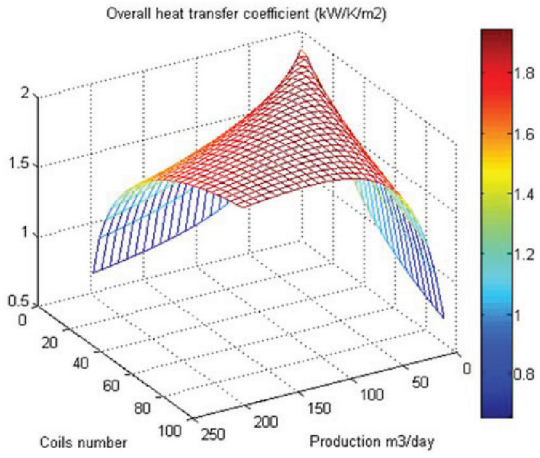

Fig. 14. The overall heat transfer coefficient vs coils number and production capacity.

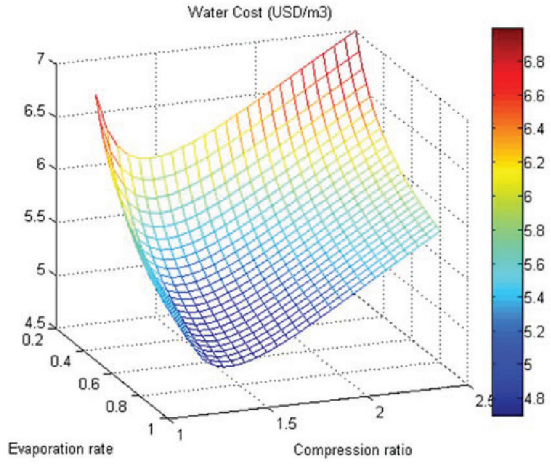

Fig. 16. Water cost (USD/m^3) vs evaporation rate and compression ratio.

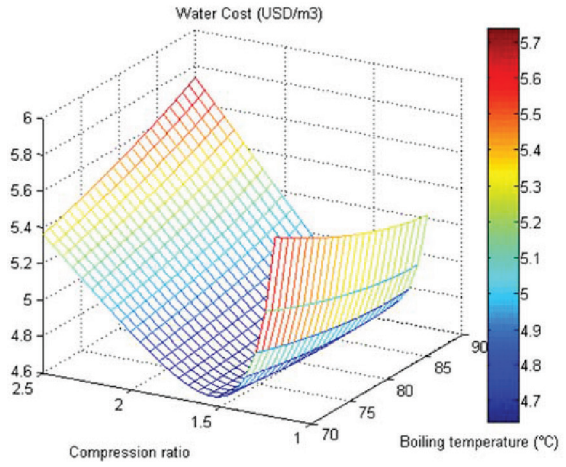

Fig. 17. Water cost (USD/m³) vs boiling temperature and compression ratio.

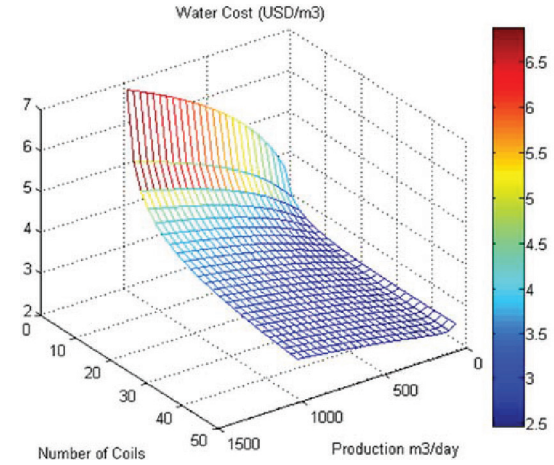

Fig. 18. Water cost (USD/m³) vs production capacity and number of coils.

and the rate of feed flowing through each heat exchanger as well as the amount of heat that should be recovered from the outlet streams. The optimization results for the recovery heat exchangers are provided in Tables 4 and 5.

6. Optimization results for multi effect-MVC unit

Previous results, dealing with single effect MVC desalination process, show that the minimum cost of water is approximately equal to 2.5 US$/m³ under strict optimization of the process. However, the average cost of water in Morocco is about 0.8 US$/m³, which is three times lower than the minimum cost of the optimized single effect MVC process configuration. Thus, this result seems to be a negative conclusion for using the MVC desalination process. However, the number of effects for such technology is a major factor for further reduction of cost and it has a direct impact on the performance of the studied desalination process.

Table 3
Thermal results for the evaporator

Production capacity (m³/d)	Overall heat transfer coefficient (kW/m²/K)	Heat transfer area (m²)	Compressor power consumption (kW)	Heat consumption (kW)
5	1.74	31	11.9	8.52
10	1.79	70.5	20.25	17.05
100	1.3	716	275	170.5
1000	1.46	3,757.0	4,642.0	1,705.0

Table 4
Heat exchanger 1 sizing results (Brine-Feed)

Production capacity (m³/d)	Overall heat transfer coefficient (kW/m²/K)	Heat transfer area (m²)	Heat recovered (kW)
5	0.85	2.19	11.1
10	1.23	3.36	24.6
100	2.13	19.38	246
1000	3	166.3	2,943.0

Table 5
Heat exchanger 2 sizing results (distilled water-feed)

Production capacity (m³/d)	Overall heat transfer coefficient (kW/m²/K)	Heat transfer area (m²)	Heat recovered (kW)
5	1.85	2.45	44.4
10	2.54	4.2	98.46
100	2.72	35	984
1000	3	292	11,774.0

Table 2
Optimal design and operational parameters for the evaporator

Production capacity (m³/d)	Optimal design and operating parameters					Cost (US$/m³)
	Compression ratio	Evaporation rate (%)	Boiling temperature (°C)	Tubes diameter (mm)	Number of coils	
5	1.4	80	75	30	5	4.2
10	1.42	80	80	30	5	3.2
100	1.57	80	82	30	10	2.54
1000	2	80	90	30	95	2.7

In this section, the developed optimization algorithm is used for different numbers of effects ranging between 1 and 14, as mentioned before, the algorithm is used to find out the most advantageous operating and design parameters leading to producing distilled water with minimized cost for various production capacities (5, 10, 100 and 1000 m^3/d). Figs. 19 and 20 illustrated results of optimization. As shown in Fig. 19, when the number of effects increases from 1 to 14, the sum of the required heat transfer areas, of all the evaporators, increases by more than 25% for each considered production capacity, while the electrical power needed for the desalination unit decreases by more than 91%. These results prove that the unit performance and cost are totally dependent and directly proportional to the number of effects. The optimized water production cost for different production capacities and different numbers of effects is shown in Fig. 20. These results prove that for a given production capacity, when the number of effects increases, the cost passes through its minimum value which corresponds to a specific number of affects and which is generally included between 6 and 8 for the considered production capacities. Indeed, the optimal number of effects is equal to 6 when the production capacity is equal to 5 m^3/d, this number increases slightly with the production capacity, to be equal to 8 when the production capacity is equal to 1000 m^3/d. Also, when the production capacity increases, the economic results presented in Fig. 20 show that the minimized cost decreases to be less than the average cost of water production in Morocco country when the production capacity is equal to 1000 m^3/d. These results prove that the mechanical vapour compression-desalination process combined with renewable energy could be a very promising in terms of performance and cost through the appropriate selection of the operating and design parameters including the number of effect and the production capacity. We recall

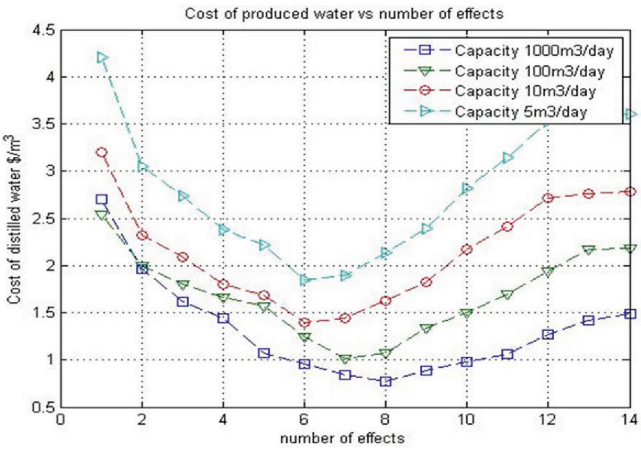

Fig. 20. Distilled water cost (US$/$m^3$) vs number of effect for different capacities (5, 10, 100 and 1000 m^3/d). These results are obtained under strict optimization of operation and design parameters using the developed optimization algorithm.

that the proposed unit uses electrical energy produced by hybrid PV-Wind energy system designed for at least ensuring 60% of fossil fuel energy replacement rate. Thus, the amount of CO_2 saving, when using the optimal number of effect, will be at least, more than 1.75, 3.81, 43.16, 219.03, and 628.3 ton/d when the production capacity is equal to 5, 10, 100 and 1000 m^3/d, respectively.

7. Exergy analysis

In earlier sections, the optimization is performed based on energy conservation law (first law of thermodynamics)

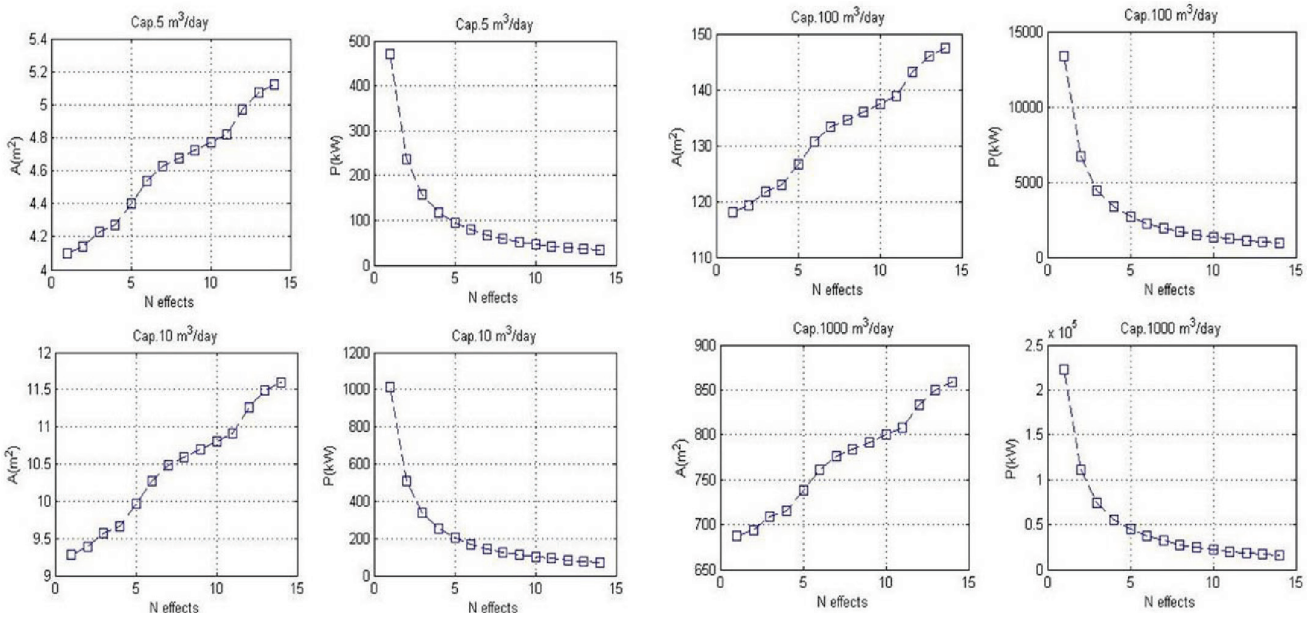

Fig. 19. Total required area of evaporators (A) and electrical power consumption (P) vs number of effect (N) for different capacities (5, 10, 100 and 1000 m^3/d). These results are obtained under strict optimization of operation and design parameters using the developed optimization algorithm.

and economic evaluation. Thus, the exergy analysis is carried out in this section in order to extend the optimization work and research for more efficient ways of using energy; for the studied desalination process; taken into account the previously obtained optimized design for each production capacity. Indeed, the exergy analysis is based on second law of thermodynamics and it allows a successful identification of locations and magnitudes of inefficient use and degradation of energy. In this section, exergy analysis is limited to evaporation/condensation unit.

The general exergy balance equation is expressed by Eq. (18):

$$\sum \dot{E}x_{in} - \sum \dot{E}x_{out} = \sum \dot{E}x_{des} \tag{18}$$

Thus, for each component in the desalination process, the exergy balance equation is modelled by Eq. (19):

$$\sum \left(1 - \frac{T_0}{T_k}\right)\dot{Q}_{net,k} - \dot{W}_{net,k} + \sum \dot{m}_{in}\psi_{in} - \sum \dot{m}_{out}\psi_{out} = \dot{E}x_{des} \tag{19}$$

where $\dot{Q}_{net,k}$ and $\dot{W}_{net,k}$ are respectively the heat transfer rate ($\dot{Q}_{out,k} - \dot{Q}_{in,k}$) and the net work transfer rate ($\dot{W}_{out,k} - \dot{W}_{in,k}$) expressed in (given in kW), the subscript '*k*' refers to a specific location in the process and subscript '0' expresses properties at the dead state (ambient/atmospheric conditions). The specific flow exergy 'ψ' (given in kJ/kg) for each flow of matter is expressed by Eq. (20):

$$\psi = (h - h_0) - T_0(s - s_0) \tag{20}$$

For incompressible processes, the specific flow exergy is modelled by Eq. (21):

$$\psi = C.\left[(T - T_0) - T_0 \ln\left(\frac{T}{T_0}\right)\right] \tag{21}$$

where 'C' is the specific thermal capacity of the substance (expressed in kJ/kg/K). The exergy balance equation for each effect number 'i' could be modelled by Eqs. (22) and (23):

For the first effect ($i = 1$):

$$\dot{E}x_{des,1} = \dot{E}x_{V_n} - \dot{E}x_{V_1} - \dot{E}x_{D_1} + \dot{E}x_{M_f} - \dot{E}x_{B_1} + \dot{E}x_{HM_{in}} - \dot{E}x_{HM_{out}} \tag{22}$$

For other effects ($i > 1$):

$$\dot{E}x_{des,i} = \dot{E}x_{V_{i-1}} - \dot{E}x_{V_i} - \dot{E}x_{D_i} + \dot{E}x_{B_{i-1}} - \dot{E}x_{B_i} \tag{23}$$

where subscripts HM_{in} and HM_{out} refer to heating medium inlet and outlet to/from the first effect. For heat recovery heat exchangers HX_1 and HX_2, the exergy balance equations could be expressed by Eq. (24):

$$\dot{E}x_{des,HX} = \dot{E}x_{cold,in} - \dot{E}x_{cold,out} + \dot{E}x_{hot,in} - \dot{E}x_{hot,out} \tag{24}$$

The exergy efficiency for each component in the desalination process could be defined as the ratio between the rate of exergy at the input and the output, thus, the exergy efficiency is defined by Eq. (25):

$$\eta_{Exergy} = \dot{E}x_{out} / \dot{E}x_{in} \tag{25}$$

The improvement potential rate (expressed in kW) is proposed by [35], this parameter is used to evaluate the maximum improvement of exergy rate that could be achieved, this means the rate of exergy destruction when exergy losses (or entropy generation) are minimized. The improvement rate (IP) is calculated for each component using Eq. (26):

$$IP = \left(1 - \eta_{Exergy}\right)\left(\dot{E}x_{in} - \dot{E}x_{out}\right) \tag{26}$$

Results presented in Table 6 show that the largest values of exergy destruction (approximately more than 20% of total exergy destruction in evaporation/condensation unit) are obtained in the first effect; indeed, the first effect exergy destruction rates for production capacities 5, 10, 100

Table 6
Obtained results for exergy destruction rates (given in kJ and in % of total)

Production capacity (m^3/d)	Exergy destruction (cap. 5 m^3/d)		Exergy destruction (cap. 10 m^3/d)		Exergy destruction (cap. 100 m^3/d)		Exergy destruction (cap. 1000 m^3/d)	
	(kW)	(% of total)	(kW)	(% of total)	(kW)	(% of total)	(kW)	(% of total)
Effect 1	0.905	20.38	2.154	24.18	20.657	30.37	200.776	26.31
Effect 2	0.814	18.33	1.539	17.28	8.933	13.13	94.761	12.42
Effect 3	0.732	16.48	1.387	15.56	8.188	12.04	86.937	11.39
Effect 4	0.662	14.89	1.254	14.04	7.512	11.04	79.678	10.44
Effect 5	0.604	13.59	1.141	12.81	6.906	10.15	73.005	9.57
Effect 6	0.559	12.58	1.051	11.80	6.376	9.37	66.944	8.77
Effect 7	–	–	–	–	5.924	8.71	61.519	8.06
Effect 8	–	–	–	–	–	–	56.760	7.44
Heat exch. I	0.152	3.42	0.339	3.81	2.955	4.34	56.760	4.46
Heat exch. II	0.014	0.32	0.041	0.46	0.550	0.81	34.033	1.12
Total	4.442	100.00	8.907	100.00	68.00	100.00	762.962	100.00

and 1000 m³/d represent respectively 20.4, 24.2, 30.4, and 26.3%. For the remaining effects, the exergy destruction rate is decreasing with the number of effect (in direction of decreasing pressure) where its percentage is ranging between 7.44 and 18.33% of the total exergy destruction rate. For heat recovery heat exchangers HX1 (distilled water/feed seawater), the exergy destruction rate represents about 3.42, 3.81, 4.34 and 4.46% for design capacities 5, 10, 100 and 1000 m3/d respectively, while the percentage of exergy destruction in HX2 (brine/feed seawater) does not exceed 1.12% of the total exergy destruction.

Figs. 21, 22 and 23 illustrate; respectively; the change of exergy destruction (kW), exergy efficiency and improvement potential rate (kW) for each component (effect 1, 2, …, n and heat exchangers "$HX1$ and $HX2$") versus the temperature difference between the first effect and the last effect in the evaporation/condensation unit ($\Delta T_t = T_1 - T_n$), ΔT_t corresponds to the last effect temperature values ranging between 40 and 65°C while the first effect temperature T_1 is kept constant and equal to the optimized value (T_1 is respectively equal to 80, 84, 75 and 85°C for desalination units with design capacities equal to 5, 10, 100 and 1000 m³/d).

Results; illustrated in Fig. 21; show that the exergy destruction rate for each effect increases as the temperature difference ΔT_t increases, however, it is slightly decreasing for heat exchangers $HX1$ and $HX2$ when ΔT_t increases. Indeed, when ΔT_t increases from 16 to 40°C, the exergy destruction rate for the first effect increases with about 30, 19, 41 and 48% for desalination units with design production capacities 5, 10, 100 and 1000 m³/d respectively, and it is increasing with more than 120% for the remaining effects and for the considered production capacities. The changes of exergy efficiency versus ΔT_t are represented in Fig. 22, it is evident from this figure that generally the exergy efficiency decreases for all components as ΔT_t increases, and it decreases very slightly for the first effect and the heat exchanger $HX1$. The influences of ΔT_t change on the improvement potential are illustrated in Fig. 23. As shown in this figure, the improvement potential for heat recovery heat exchangers $HX1$ and $HX2$ decreases with very small rate as ΔT_t increases. The highest values of the improvement potential are recorded for the first effect for all considered production capacities, and it has approximately the same values for the remaining effect. Also, Fig. 23 demonstrated that the improvement potential for all effects increases when ΔT_t increases.

Generally, the exergy destruction rate (irreversibility or entropy generation) could be minimized by adopting small values of temperature difference between the first and the last effect; however, this leads to decreasing the temperature differences between fluids exchanging heat inside each effect (ΔT_i) and in the same time it causes a reduction of the global heat transfer coefficients and consequently it causes the increase of the required heat transfer area inside each effect. In addition, decreasing exergy destruction rate by decreasing ΔT_t will result on decreasing the pressure ratio for the compressor and therefore, it will result on reducing the specific energy consumption.

8. Conclusion

The main objective of this work is to provide detailed sizing model, thermal and economic analysis, optimization procedure and their results, of seawater desalination process based on mechanical vapour compression process combined with renewable energy sources, in order to

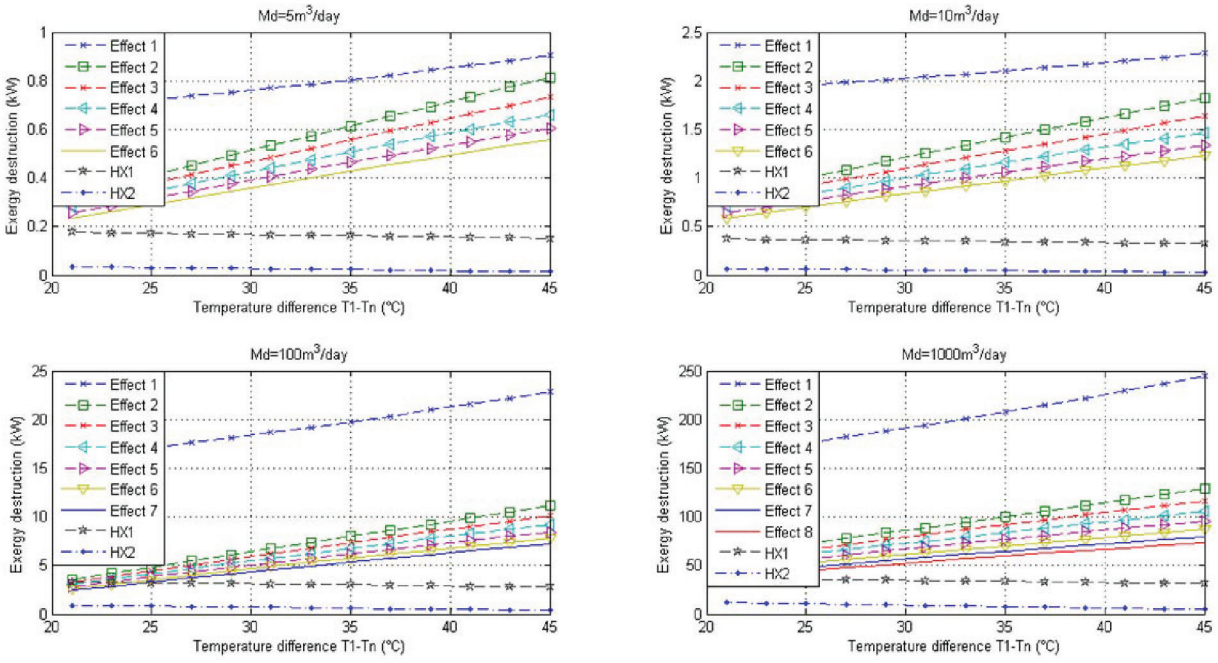

Fig. 21. Exergy destruction rate variation (kW) for different design capacities (5, 10, 100 and 1000 m³/d) vs temperature difference change $\Delta T_t = T_1 - T_n$ (°C).

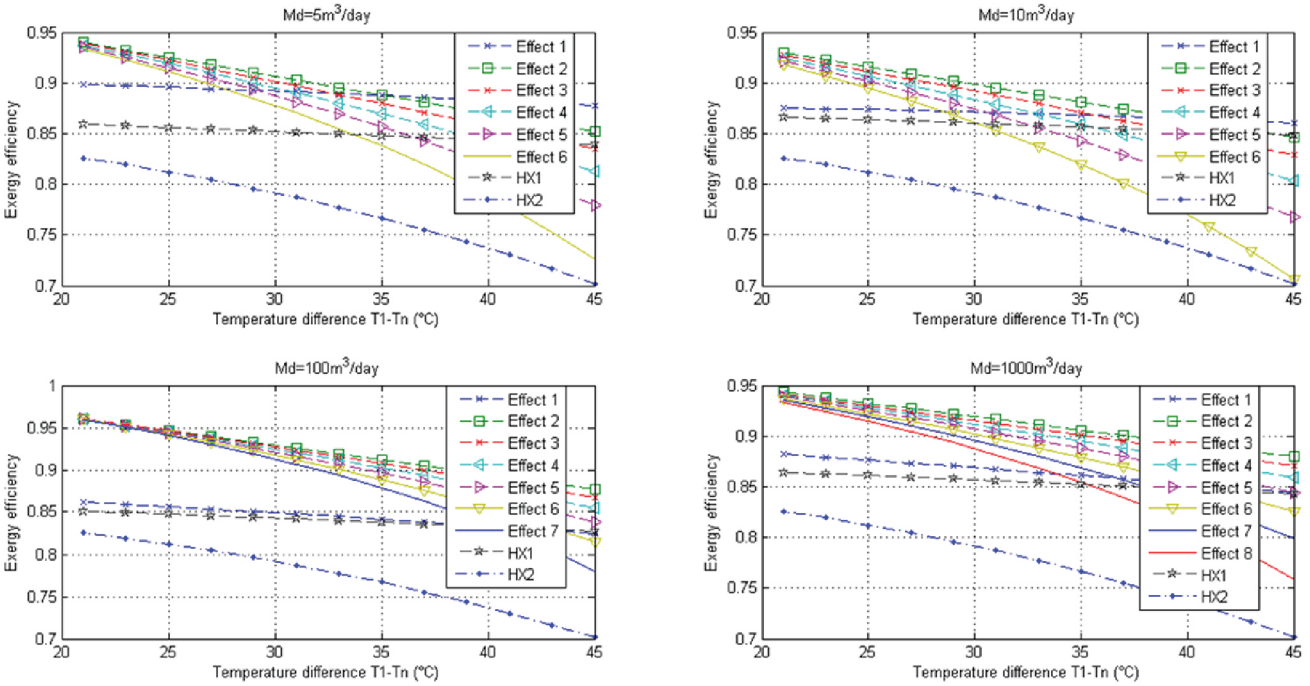

Fig. 22. Exergy efficiency change for different design capacities (5, 10, 100 and 1000 m³/d) vs temperature difference change $\Delta T_t = T_1 - T_n$ (°C).

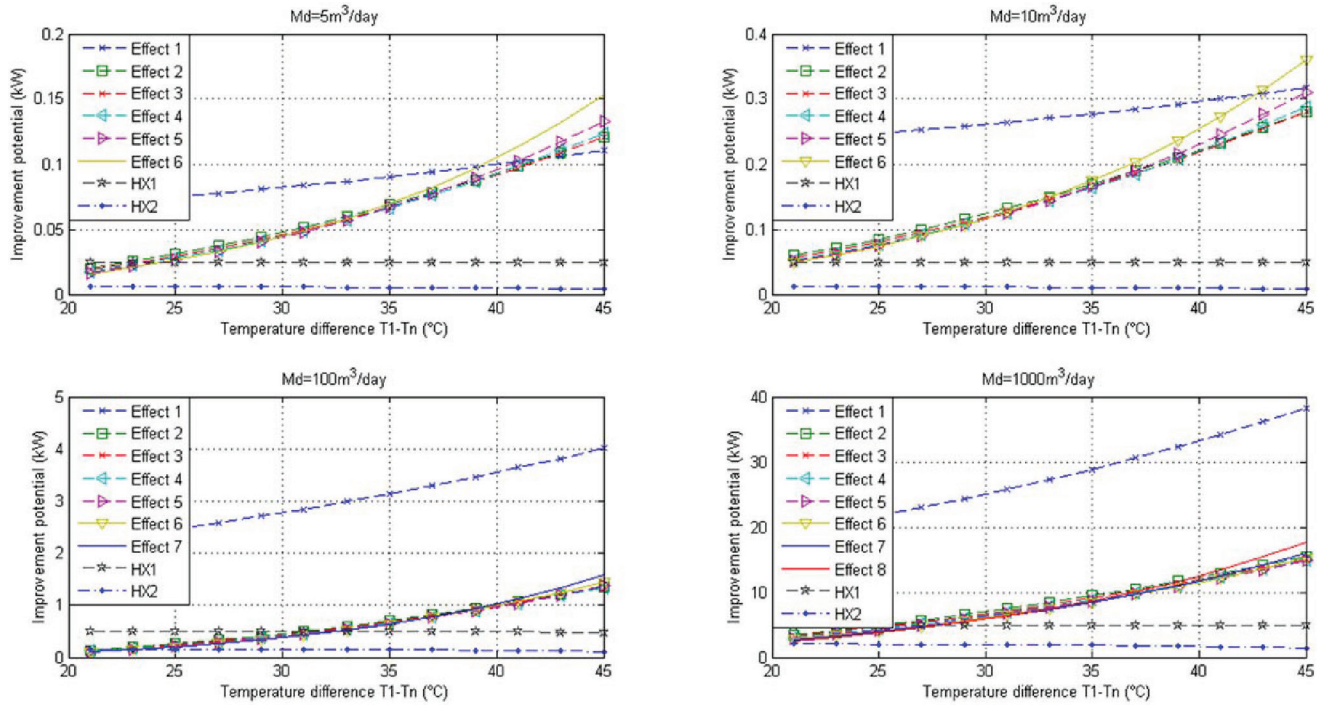

Fig. 23. Improvement potential rate variation for different design capacities (5, 10, 100 and 1000 m³/d) vs temperature difference change $\Delta T_t = T_1 - T_n$ (°C).

evaluate the effectiveness and the performance of such process in terms of cost and environment protection. The developed model is based on energy balance equations, heat transfer and thermodynamic correlations in addition to other technical and engineering relationships related to each component. The developed sizing model is resolved using fixed point iteration method, implemented using Matlab programming software, and validated based on

published data of the Heat Transfer Laboratory of the Atomic Energy Authority of Egypt. The thermal and economic analyses take into account the effect of design and operating parameters on the unit performance. The optimization procedure uses genetic algorithm method, in order to find out the most advantageous design and operating parameters for different number of effects and different production capacities leading to produce distilled water with minimized cost. Genetic Algorithm is also applied to optimize the hybrid Wind-photovoltaic energy system configuration and sizing.

Results of this work prove that under strict optimization, the desalination process using multi-effect mechanical vapour compression process could very promising way to deal with water shortage with a reasonable cost which could be less than the average cost of water production in Morocco. Indeed, the obtained results show that the cost of water produced using vapour compression process with single effect is not competitive even under strict optimization of the unit, however, it could be reduced notably by selecting the appropriate number of effect; and increasing the production capacity to be less than 0.8 US$/m^3. Another advantage of the proposed technology is the integration of renewable energy sources which could allow a considerable reduction of CO_2 emissions.

This study is completed with exergy analysis efficiency in order to discuss other possibilities to improve the studied desalination process. The exergy efficiency analysis proves that the rate of entropy generation (exergy destruction) could be minimized by reducing the total temperature difference between the first effect and the last one, which result on increasing the required heat transfer for each effect while it helps on reducing the specific energy consumption for the compressor.

Appendix

1. Optimal configuration of hybrid PV-wind energy system – Case study: Laayoune region

The aim of the optimization procedure of the hybrid wind-PV system is to find out the optimal configuration of the hybrid system in terms of contribution rate of each source of energy and batteries size leading to producing electrical energy with minimized cost, satisfying the energy load and ensuring the required fossil fuel replacement rate. Three complementary steps are used in the optimization procedure, which are:

- Prediction of the monthly average weather data of the selected location (Laayoune region (33°39′58″ N, 7°04′16″ W)-Morocco);
- Sizing each renewable energy technology based on a typical production load of 1MW;
- Applying Genetic optimization algorithm to find out the contribution rate of each technology in terms of sizing.

1.1. Meteorological data

The monthly average solar energy flux profile during one year is estimated using El Mghouchi model as described in reference [25], while the monthly average wind velocity profile during one year is obtained from reference [26]. These two data are collected and presented in Fig. 24.

1.2. Sizing methodology and results for each technology for 1 MW as maximum power load

Photovoltaic panels and wind turbines are designed for a maximum production load of P_{load} = 1 MW, thus the sizing calculations are based on the period in which the natural source potential is maximum during a year (maximum wind velocity and solar irradiation. The required area of the photovoltaic panels ($A_{PV} = N_{panels} * A_{panel}$) is calculated using equation:

$$A_{PV} = P_{load} \Big/ \left(E_g \eta_{PV} PR_{pv} \right) \tag{27}$$

where η_{PV} and PR_{PV} are, respectively, the panels efficiency, and the performance ratio. The *PV* panel cost in Morocco is estimated equal to 700 US$ (with an absorber area equals to 1.65 m^2/panel), it is determined based on the actual

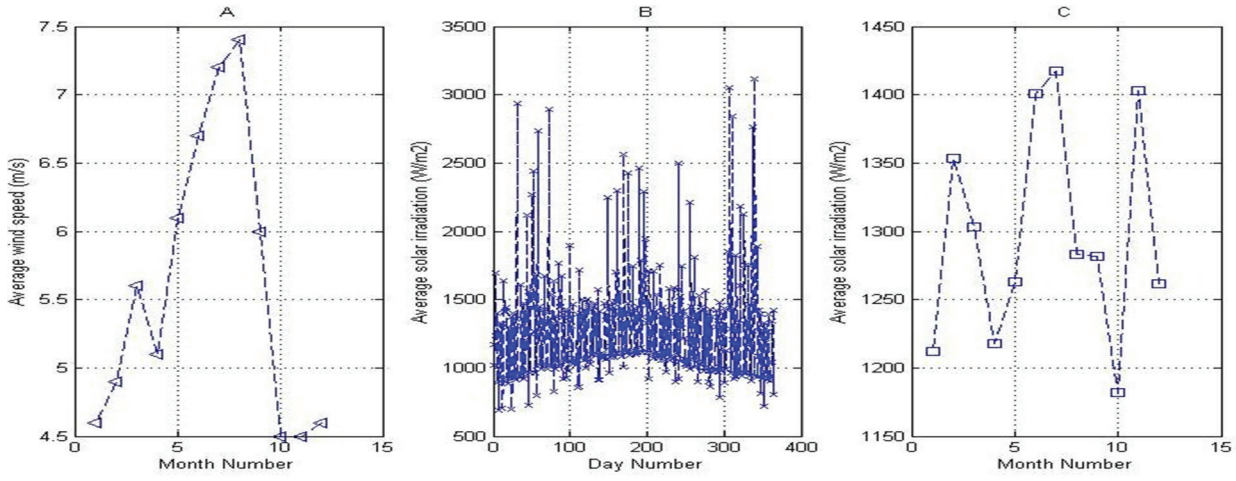

Fig. 24. Average wind speed (m/s) and solar irradiation (W/m2) during a year for Laayoune region-Morocco.

situation of the market. The annual maintenance cost for each PV panel is taken equal to 14 US$. The total power output of wind turbines depends on wind velocity and their technical characteristics, which are: cut-in speed (v_c = m/s), cut-off speed (v_f = m/s), rated speed (v_r = m/s) and rated power (P_r = kw).

For a single wind turbine, the electrical power output is given by the following equations [23]:

$$P_W = \begin{cases} 0 \; if \; v > v_f \; or \; v < v_c \\ P_r\left(av^3 - b\right) if \; v_c < v < v_r \\ P_r \; if \; v_r < v < v_f \end{cases} \quad (28)$$

where parameters '*a*' and '*b*' are calculated as in reference [23]. The investment cost for wind turbines is equal to 3200 US$, and the annual maintenance cost is estimated equal to 100 USD [27]. Life time of the hybrid renewable energy system is taken equal to 25 years and 5% is assumed for the interest rate. Results of the initial sizing of both Wind and PV system for a maximum power output of 1 MW are presented in Fig. 25. These results are: the electrical power output, energy produced per month and the energy cost.

1.3. Optimization procedure and problem formulation

As mentioned before, the objective is to find out the most advantageous configuration of the energy hybrid system in terms of sizing contribution of each considered technology. The objective function to minimize is defined as:

$$f_{\min}(cost) = \min \begin{pmatrix} \Sigma_{i=1}^{12}\left(\Sigma_{j=1}^{24}\left(X_{i,j}^{PV} Y_{PV} C_{i,PV} E_{i,PV} + X_{i,j}^{W} Y_W C_{i,W} E_{i,W}\right.\right. \\ \left.\left. + X_{i,j}^{Up} C_{Up} E_{Up} + X_{i,j}^{disch} C_{i,j}^{disch} E_{i,j}^{Batt}\right.\right. \end{pmatrix} \quad (29)$$

The total load 'E_{load} = 1 MWh' of energy must be satisfied during each hour, thus, the first equality constraint is expressed by:

$$E_{load} = X_{i,j}^{PV} Y_{PV} E_{i,PV} + X_{i,j}^{W} Y_W E_{i,W} + X_{i,j}^{Up} E_{Up} + X_{i,j}^{disch} E_{i,j}^{Batt} \quad (30)$$

Also, the hybrid system must ensure at least 60% of fossil fuel replacement rate, thus the first inequality constraint is expressed by:

$$\Sigma_{j=1}^{24}\left(0.6E_{load} - \begin{pmatrix} X_{i,j}^{W} Y_{PV} E_{i,PV} + X_{i,j}^{W} Y_W E_{i,W} \\ + X_{i,j}^{disch} E_{i,j}^{Batt} \end{pmatrix}\right) \le 0 \quad (31)$$

The batteries storage state must be always less than its maximum value and the amount of energy that could be discharged must be always less or equal to the available energy, thus the two other inequality constraints related to batteries are expressed by the following:

$$E_{i,j}^{Batt} \le E_{\max}^{Batt} \quad (32)$$

$$X_{i,j}^{disch} E_{i,j}^{Batt} \le E_{i,j}^{Batt} - E_{\min}^{Batt} \quad (33)$$

In order to avoid the energy losses, all the renewable energy produced must be used or stored in the batteries, thus, the second equality constraint is expressed by:

$$E_{i,j}^{Batt} - E_{i,j}^{Batt} = \left(1 - X_{i,j}^{PV}\right) Y_{PV} E_{i,PV} + \left(1 - X_{i,j}^{W}\right) Y_W E_{i,W} \quad (34)$$

The cost of energy discharged from batteries is calculated based on the cost of energy charged and the batteries investment cost, thus it is evaluated using equation:

$$C_{i,j}^{disch} = C_{i,j}^{ch} + C_{batt}^{inv} \quad (35)$$

where the energy charging cost is estimated by:

$$C_{i,j}^{ch} = A_1 / A_2 \quad (36)$$

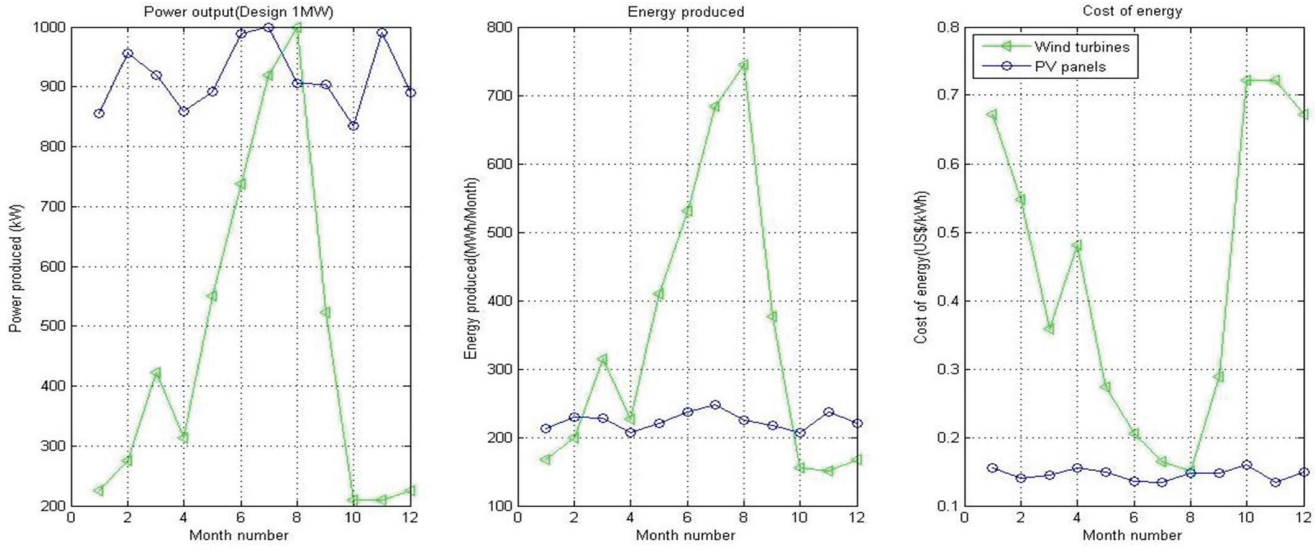

Fig. 25. Sizing results of wind turbines and PV panels (for 1MW)-power output (kW), energy produced per month (MWh/month) and cost of energy (US$/kWh).

where A_1 and A_2 are expressed by the following equations:

$$A_1 = \left(C_{i,j-1}^{ch} E_{i,j-1}^{Batt} + \begin{pmatrix} \left(1 - X_{i,j}^{W}\right) C_{i,PV} Y_{PV} E_{i,PV} \\ + \left(1 - X_{i,j}^{W}\right) C_{i,W} Y_W E_{i,W} \end{pmatrix} \right) \quad (37)$$

$$A_2 = \left(E_{i,j-1}^{Batt} + \left(\left(1 - X_{i,j}^{W}\right) Y_{PV} E_{i,PV} + \left(1 - X_{i,j}^{W}\right) Y_W E_{i,W} \right) \right) \quad (38)$$

The resolution and optimization algorithm is based on using Genetic algorithm optimization method as shown in Fig. 26. The first step is generating randomly an initial population of variables, which are: the energy contribution of each source of energy including the energy storage system ($X_{i,j}^{W}$; $X_{i,j}^{PV}$; $X_{i,j}^{disch}$; and $X_{i,j}^{Up}$), the contribution of each renewable energy source in terms of design compared to the initial sizing, which are : Y_{PV} and Y_W, and the maximum storage capacity of batteries. Then, the equality and inequality constraints are evaluated. If any of the initial generated solutions violates the problem constraints then it is replaced by a new one selected randomly.

The second step is the fitness function evaluation for each feasible solution in the selected population, which is the energy cost equation to minimize. The fitness function with lowest value compared to the value obtained from the previous iterations is considered as an initial optimal solution of the optimization algorithm. The initial-best solutions create the next generation through the selection of chromosomes, crossover and mutation operations. The same procedure is repeated until achieving the maximal number of iterations. Also, the algorithm stops if there are no improvements of the value of the fitness function after a set number of generations.

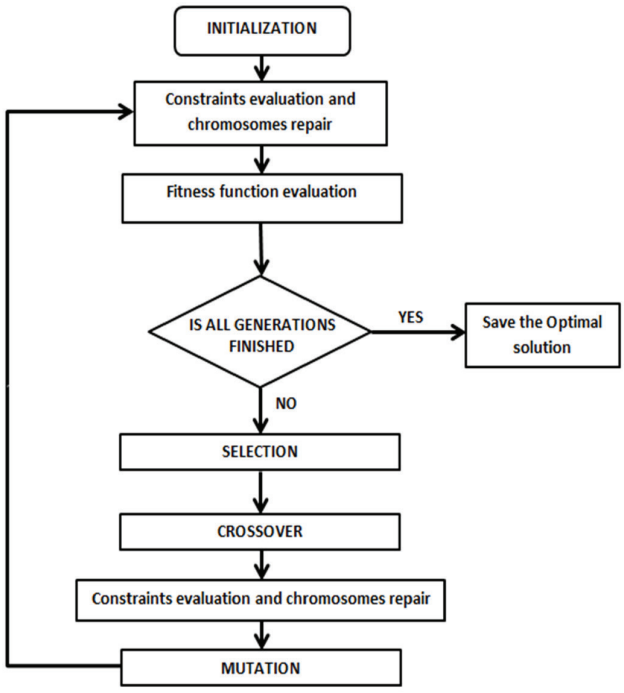

Fig. 26. Simplified schematic of Genetic algorithm applied for the hybrid wind-PV system.

The optimal results for the energy production system are given in the Table 7 for a typical electrical power production of 1MW.

2. Convective heat transfer coefficient for plate heat exchangers

To evaluate the convective heat transfer coefficient he most widely used plates has the following relationship for the turbulent flow [28]:

$$\mathrm{Nu} = 0,374\,\mathrm{Re}^{0,668}\,\mathrm{Pr}^{0,33}\left(\mu_b / \mu_w\right)^{0,15} \quad (39)$$

where the Reynolds number is based on equivalent diameter, De, defined by

$$D_e = \frac{4Wb}{2(W+b)} = 2b \quad (40)$$

Because b is very small compared to W.
For laminar flow:

$$\mathrm{Nu} = c_1\left(\mathrm{Re}\frac{\mathrm{Pr}\,D_e}{L}\right)^{0,333}\left(\mu_b / \mu_w\right)^{0,14} \quad (41)$$

where c_1 = 1.86–4.50 depending on geometry, and L is the effective plate length. Dimensions W, L, $X1$, $X2$ and b are shown in Fig. 27.

Table 7
Summary of optimization sizing results

Y_{PV} (%)	60
Y_W (%)	70
Batteries capacity (kWh)	20
Cost of energy (US$/kWh)	0.14
Fossil fuel replacement (%)	63
CO_2 emissions saving (ton/MWh)	5,192

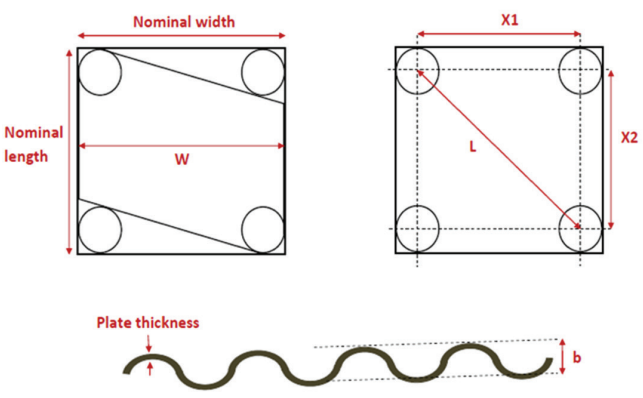

Fig. 27. Plate dimensions-Plate heat exchanger.

3. Boiling heat transfer coefficient at the outside of submerged coil

Schrock-Grassman's correlation [29] is used to predict the boiling heat transfer coefficients of boiling seawater in contact with the outside heat transfer area of coils located at upper part of the evaporator. The convective heat transfer coefficient in this case is calculated by:

$$h_b = 170\frac{\lambda_l}{d}\mathrm{Re}_{l0}^{0.8}\,\mathrm{Pr}^{1/3}\left(B_0 + 1.510^{-4}X_{tt}^{-0.67}\right) \tag{42}$$

$$B_0 = q/Gr \tag{43}$$

$$\mathrm{Re}_{l0} = dG/\mu_l \tag{44}$$

$$\frac{1}{X_{tt}} = \left(\frac{x}{1-x}\right)^{0.9}\left(\frac{\rho_l}{\rho_g}\right)^{0.5}\left(\frac{\mu_g}{\mu_l}\right)^{0.1} \tag{45}$$

4. Condensing heat transfer coefficient inside a coil

The condensation heat transfer coefficient for water vapour flowing inside helical coil tube is related to the condensation heat transfer coefficient when using vertical tube by the equation presented by Kern [24].

$$\mathrm{h}_{\mathrm{coil}} = \left(1 + 3.5\frac{d_i}{D_h}\right)h_{vertical} \tag{46}$$

The condensation heat transfer coefficient could be estimated using equation:

$$h_{vertical} = 0,925\left(\rho_L^2 g n\pi D_{in}/\mu_L W_L\right)^{1/3} \tag{47}$$

5. Convective heat transfer coefficient for liquid water flowing inside and outside a coil

One of the more accurate correlations used to calculate the convective heat transfer coefficient for liquid flowing inside a helical coil is given by Petukhov [24]. The correlation is valid for $0.5 < \mathrm{Pr} < 2.10^3$ and $10^4 < \mathrm{Re} < 5.10^6$:

$$h_i = \left(\frac{f}{2}\right)D^{-1}\mathrm{Re}\,\mathrm{Pr}\,k_i\left(1.07 + 12.7\left(\frac{f}{2}\right)^2\left(\mathrm{Pr}^{\frac{2}{3}} - 1\right)\right) \tag{48}$$

where f is the friction factor which can be calculated using equation (49)

$$f = \left(1.85\ln(\mathrm{Re}) - 3.28\right)^{-2} \tag{49}$$

For laminar flow, the Sieder and Tate correlation can be used as expressed by Eq. (50).

$$h_i = 1.86k_iD^{-1}\left(\mathrm{Pr}\,\mathrm{Re}\,DL^{-1}\right)^{1/3} \tag{50}$$

The heat transfer coefficient is then corrected using the coil dimensions by the equation below: equation is applicable for 0, $84 < \mathrm{Pr} < 16700$ and $(\mathrm{Re}\,\mathrm{Pr}\,D/L) > 2$.

$$\mathrm{h}_{\mathrm{icoil}} = h_i\left(\frac{D}{d_0}\right) \tag{51}$$

6. Convective heat transfer coefficient from submerged coil

The outside heat transfer coefficient is calculated in function of Rayleigh number using the length of the tube as the characteristic length based on the Nusselt number [24].

$$Nu_L = 0.685Ra_L{}^{0.295} \tag{52}$$

This formula is valid when $3.10^{12} < \mathrm{Ra_L} < 8.10^{14}$

$$Nu_L = 0.00044Ra_L{}^{0.516} \tag{53}$$

This formula is valid when $6.10^{11} < \mathrm{Ra_L} < 1.10^{14}$

7. Correlation used to calculate the thermodynamics properties of streams [30,31]

7.1. Boiling point elevation

The boiling point rise caused by the salinity (BPE) and the hydrostatic head is given by the equation:

$$T_i = T_{vi} + (BPE)_i + \Delta T_{hi} \tag{54}$$

The boiling point rise caused by the salinity (BPE) can be calculated as a function of temperature and concentration of salt. Accordingly,

$$BPE = Ac + Bc^2 \tag{55}$$

where A and B are temperature dependent constants, calculated by the following:

$$A = A_1 + A_2t + A_3t^2 \tag{56}$$

$$B = B_1 + B_2t + B_3t^2 \tag{57}$$

The coefficients Ai and Bi are given as the following:

$\mathrm{A_1} = 0.2009 \times 10^{-3}$ $\quad \mathrm{B_1} = 0.0257 \times 10^{-3}$

$\mathrm{A_2} = 0.2867 \times 10^{-5}$ $\quad \mathrm{B_2} = 0.0193\times 10^{-5}$

$\mathrm{A_3} = 0.0020 \times 10^{-7}$ $\quad \mathrm{B_3} = 0.0001\times 10^{-7}$

where the concentration c is expressed by the chlorinity factor and the temperature is expressed in (°C).

7.2. Latent heat of evaporation/condensation

The latent heat of evaporation (or condensation) of water can be expressed as a function of temperature by the following expression:

$$L = 2499,5698 - 2,204864T - 1,59610^{-3}T^2 \quad (58)$$

where T is the saturation temperature in °C and l is the latent heat in kJ/kg.

7.2.1. Specific thermal capacity

The seawater specific heat at constant pressure is given by the following correlation:

$$C_p = \left(\alpha_0 + \alpha_1 T + \alpha_2 T^2 + \alpha_3 T^3\right)10^{-3} \quad (59)$$

where α_0, α_1, α_2, α_3 are salt concentration dependent constants, calculated by the following:

$\alpha_0 = 4206,8 - 6,6197c + 1,228810^{-2}c^2$

$\alpha_1 = -1,1262 + 5,417810^{-2}c - 2,271910^{-4}c^2$

$\alpha_2 = 1,202610^{-2} - 5,356610^{-4}c + 1,890610^{-6}c^2$

$\alpha_3 = 6,877710^{-7} + 1,51710^{-6}c - 4,426810^{-9}c^2$

This correlation is valid over salinity between 20,000 and 160,000 ppm and temperature ranges between 20 and 180°C.

7.3. Seawater dynamic viscosity

The dynamic viscosity of seawater is given by the correlation bellow:

$$\mu = 10^{-3}\mu_W\mu_R \quad (60)$$

With:

$$\mu_W = \exp\left(-3,79418 + \frac{604,129}{(139,18 + T)}\right) \quad (61)$$

$$\mu_R = 1 + \beta_1 c + \beta_2 c^2 \quad (61a)$$

$$\beta_1 = 1,47410^{-3} + 1,510^{-5}\mathrm{T} - 3,92710^{-8}\mathrm{T}^2 \quad (62)$$

$$\beta_2 = 1,07310^{-5} - 8,510^{-8}T + 2,2310^{-10}T^2 \quad (63)$$

where μ is in kg/m s, T is in °C, and c is in gm/kg.

The above correlation is valid over salinity range between 0 and 130 gm/kg and temperature range between 10 and 180°C.

7.4. Other properties

The thermal capacity, density, thermal conductivity and the relationship between steam temperature and pressure of saturation are determined using the correlations presented in the appendix of reference [20].

8. Different costs calculation

8.1. Evaporator cost

The evaporator cost is related to its heat transfer area, the economic model proposed by [32] is used in this study to estimate the purchase and the installation cost of the evaporator in US$:

$$C_{evap} = 0,009079\left\{\begin{matrix}\left[4400 + (B - 620)\right] \times 1,2 \\ \times (0,667 + 0,0287 \times A) \times h\end{matrix}\right\} \quad (64)$$

where B is the material price of the evaporator, h is the gain coefficient and A is the surface area of the evaporator.

8.2. Compressor and pumps

The compressor and pumps cost is calculated using the equations provided by [33]. For the compressor, the investment cost is determined by:

$$C_{comp} = 736\dot{M}_v\left(\frac{P_0}{P_i}\right)\left(\eta_c \big/ 1 - \eta_c\right)^{0.7} \quad (65)$$

where M_v is the mass flow rate of vapour (kg/s), P_o and P_i are respectively the pressure at the outlet and the inlet of the compressor and η is the compressor efficiency.

For the pump, the cost could be estimated using the equation

$$C_{pump} = 13.92\dot{M}_w{}^{0.5}\Delta P^{0.5}\left(\eta \big/ 1 - \eta\right)^{1.5} \quad (66)$$

where M_w is the mass flow rate of the liquid pumped (kg/s), ΔP is the pressure lost inside the pipe (kPa) and η is the pump efficiency.

C_{comp} and C_{pump} are given in US Dollar.

8.3. Heat exchangers cost

The cost equation presented in [34] is used to estimate the investment cost for the plate heat exchangers (US Dollar).

$$\mathrm{C_{hexchanger}} = 1000\left(12.86 + A^{0.8}\right) \quad (67)$$

where A is the required heat transfer area (m^2).

8.4. Tanks, pipes, connections Maintenance and other auxiliary material

The rates of the other different costs (% of the capital cost) are summarized as following:

- Tanks, piping and valves (4%)
- Maintenance and cleaning (3%)

- Manpower (2%)
- Spare parts (1%)

9. Amortization

The annual amortization factor F is determined using the relationship:

$$F = \frac{i(1+i)^n}{(1+i)^n - 1} \tag{68}$$

The annual amortization is taken the same for all the unit components. The interest rate is taken equal to 5% and 25 years is considered for the amortization.

Acknowledgment

The authors of this paper acknowledge the financial support by "Institute for Research in Solar Energy and New Energies, IRESEN" of the "Seawater desalination using solar energy" project.

Symbols

m — Mass flow rate (kg/s)
X — Evaporation rate (%)
T — Temperature (°C)
C — Thermal capacity (kJ/kg/°C)
U — Overall heat transfer coefficient (kW/m^2/°C)
h — Convective heat transfer coefficient (kW/m^2/°C)
A — Heat transfer area (m^2)
L — Latent heat (kJ/kg)
Eg — Solar irradiation (W/m^2)
P — Pressure (kPa)
v — Specific volume (kg/m^3)
D — Coil diameter (m)
d — Tube diameter (m)
Re — Reynolds number
Pr — Prendtl number
Ra — Rayleigh number
Nu — Nusselt number
C — Cost (USD)
$\dot{E}x$ — Flow exergy rate (W or kW)
ψ — Specific exergy rate (J/kg or kJ/kg)
IP — Improvement potential (W or kW)
F — Amortization factor (%)
i — Interest rate (%)
n — Number of years

Greek

α — Heat exchangers feed fraction
γ — Rayleigh number
μ — Dynamic viscosity
η — Efficiency (%)
Δ — Difference
λ — Thermal conductivity (kJ/m/°C)
ρ — Density (kg/m^3)

Subscripts

b — Rejected brine
d — Distillate
f — Feed seawater
h — Heating
i — Inlet
o — Outlet
pv — Photovoltaic
st — Solar thermal
v — Vapour
evap — Evaporator
comp — Compressor
r — Recovery
los — Lost

Abbreviations

MVC — Mechanical vapour compression
HE — Heat exchanger
TVC — Thermal vapour compression
LMTD — Log mean temperature difference
OHTC — Overall heat transfer coefficient
HTA — Heat transfer area
MED — Multi effect evaporation/distillation
USD — United State Dollar

References

[1] K. Tahri, Desalination experience in Morocco, Desalination, 136 (2001) 43–48.
[2] R. Matz, U. Fisher, A comparison of the relative economics of sea water desalination by vapor compression and reverse osmosis for small to medium capacity plants, Desalination, 36 (1981) 137–151.
[3] M.A. Darwish, Thermal analysis of vapor compression desalination system, Desalination, 69 (1988) 275–295.
[4] O.A. Hamed, A.M. Zamamiri, S. Aly, N. Lior, Thermal performance and exergy analysis of a thermal vapor compression desalination system, Energy Conv. Manage., 37 (1996) 379–387.
[5] F. Al-Juwayhel, H. El-Dessouky, H. Ettouney, Analysis of single-effect evaporator desalination systems combined with vapor compression heat pumps, Desalination, 114 (1997) 253–275.
[6] H. Ettouney, H. El-Dessouky, Y. Al-Roumi, Analysis of mechanical vapour compression desalination process, Int. J. Energy Res., 23 (1999) 431–451.
[7] H.S. Aybar, Analysis of a mechanical vapor compression desalination system, Desalination, 142 (2002) 181–186.
[8] J.R. Lara, G. Noyes, M.T. Holtzapple, An investigation of high operating temperatures in mechanical vapor-compression desalination, Desalination, 227 (2008) 217–232.
[9] J. Ji, R. Wang, L. Li, H. Ni, Simulation and analysis of single effect thermal vapour compression desalination system at variable operating conditions, Chem. Eng. Technol., 30 (2007) 1633–1641.
[10] A.S. Nafey, H.E.S. Fath, A.A. Mabrouk, Thermoeconomic design of a multi-effect evaporation mechanical vapor compression (MEE–MVC) desalination process, Desalination, 230 (2008) 1–15.
[11] M.A. Sharaf, A.S. Nafey, L.G. Rodríguez, Thermo-economic analysis of solar thermal power cycles assisted MED-VC (multi effect distillation-vapor compression) desalination processes, Energy, 36 (2011) 2753–2764.
[12] J. Shen, Z. Xing, X. Wang, Z. He, Analysis of a single-effect mechanical vapor compression desalination system using water injected twin screw compressors, Desalination, 333 (2014) 146–153.

[13] A. Kouta, F. Al-Sulaiman, M. Atif, S. Bin Marshad, Entropy, exergy, and cost analyses of solar driven cogeneration systems using supercritical CO_2 Brayton cycles and MEE-TVC desalination system, Energy Convers. Manage., 115 (2016) 253–264.
[14] M. Lucas, B. Tabourier, The mechanical vapour compression process applied to seawater desalination : a 1,500 ton/day unit installed in the nuclear power plant of Flamanville, France, Desalination, 52 (1985) 1123–133.
[15] Z. Zimerman, Development of large capacity high efficiency mechanical vapor compression (MVC) units, Desalination, 96 (1994) 51–68.
[16] J.M. Veza, Mechanical vapour compression desalination plants-A case study, Desalination, 101 (1995) 1–10.
[17] A. Karameldin, A. Lotfy, S. Mekhemar, The Red Sea area wind-driven mechanical vapor compression desalination system, Desalination, 153 (2002) 47–53.
[18] Narmine H. Aly, Adel K. El-Fiqi, Mechanical vapor compression desalination systems-a case study, Desalination, 158 (2003) 143–150.
[19] R. Bahar, M.N.A. Hawlader, L.S. Woei, Performance evaluation of a mechanical vapor compression desalination system, Desalination, 166 (2004) 123–127.
[20] A.M. Helal, S.A. Al-Malek, Design of a solar-assisted mechanical vapor compression (MVC) desalination unit for remote areas in the UAE, Desalination, 197 (2006) 273–300.
[21] Y.M. El-Sayed, Thermoeconomics of some options of large mechanical vapor-compression units, Desalination, 125 (1999) 251–257.
[22] M. Khayet, Solar desalination by membrane distillation: Dispersion in energy consumption analysis and water production costs (a review), Desalination, 308 (2013) 89–101.
[23] D. Zejli, A. Ouammi, R. Sacile, H. Dagdougui, A. Elmidaoui, An optimization model for a mechanical vapor compression desalination plant driven by a wind/PV hybrid system, Appl. Energy, 88 (2011) 4042–4054.
[24] D.Q. Kern: Process Heat Transfer, McGraw-Hill, 1965.
[25] Y. El Mghouchi, A. El Bouardi, Z. Choulli, T. Ajzoul, New model to estimate and evaluate the solar radiation, Int. J. Sustain. Built Environ., 3 (2014) 225–234.
[26] H. Nfaoui, J. Bahrau, A.S. Darwish, A.A.M. Sayigh, Wind energy potential in Morocco, Renew. Energy, 1 (1991) 1–8.
[27] D.B. Nelson, M.H. Nehrir, C. Wang, Unit sizing and cost analysis of stand-alone hybrid wind/PV/fuel cell power generation systems, Renew. Energy, 31 (2006) 1641–1656.
[28] M.B. Kumbhare, S.D. Dawande, Performance evaluation of plate heat exchanger in laminar and turbulent flow conditions, Int. J. Chem. Sci. Appl., 4 (2013) 77–83.
[29] H. Nariai, Friction Pressure Drop and heat transfer coefficient of two-phase flow in helically coiled tube once-through steam generator for integrated type marine water reactor, J. Nucl. Sci. Technol., 19 (1982) 936–947.
[30] B. Fabuss, A. Korosi, Boiling point elevations of seawater and it concentrates, J. Chem. Eng. Data, 11 (1966) 606–609.
[31] H. El-Dessouky, H.M. Ettouney, Fundamentals of Salt Water Desalination. Elsevier, Amsterdam, 2002.
[32] X. Liu, W. Chen, M. Gu, S. Shen, G. Cao, Thermal and economic analyses of solar desalination system with evacuated tube collectors, Solar Energy, 93 (2013) 144–150.
[33] Y.M. El-Sayed, Designing desalination systems for higher productivity, Desalination, 134 (2001) 129–159.
[34] W. El-Mudir, M. El-Bousiffi, S. Al-Hengari, Performance evaluation of a small size TVC desalination plant, Desalination, 165 (2004) 269–279.
[35] F. Balkan, N. Colak, A. Hepbasli, Performance evaluation of a triple-effect evaporator with forward feed using exergy analysis, Int. J. Energy Res., 29 (2005) 455–470.